Molecular model of fission yeast centrosome assembly determined by superresolution imaging

Andrew J. Bestul,[1] Zulin Yu,[1] Jay R. Unruh,[1] and Sue L. Jaspersen[1,2]

[1]Stowers Institute for Medical Research, Kansas City, MO
[2]Department of Molecular and Integrative Physiology, University of Kansas Medical Center, Kansas City, KS

Microtubule-organizing centers (MTOCs), known as centrosomes in animals and spindle pole bodies (SPBs) in fungi, are important for the faithful distribution of chromosomes between daughter cells during mitosis as well as for other cellular functions. The cytoplasmic duplication cycle and regulation of the *Schizosaccharomyces pombe* SPB is analogous to centrosomes, making it an ideal model to study MTOC assembly. Here, we use superresolution structured illumination microscopy with single-particle averaging to localize 14 *S. pombe* SPB components and regulators, determining both the relationship of proteins to each other within the SPB and how each protein is assembled into a new structure during SPB duplication. These data enabled us to build the first comprehensive molecular model of the *S. pombe* SPB, resulting in structural and functional insights not ascertained through investigations of individual subunits, including functional similarities between Ppc89 and the budding yeast SPB scaffold Spc42, distribution of Sad1 to a ring-like structure and multiple modes of Mto1 recruitment.

Introduction

Inside of cells, the spatial and temporal organization of microtubules is governed by a diverse group of structures known as microtubule-organizing centers (MTOCs). The common feature of all MTOCs is their ability to recruit γ-tubulin complexes (γ-TCs), which form a template for microtubule growth (Kollman et al., 2011). During mitosis, centrosomes (metazoans) or spindle pole bodies (SPBs; fungi) function as MTOCs, forming the poles of the mitotic spindle. Much like genome replication, duplication of the centrosome/SPB is tightly regulated with the cell cycle to ensure the formation of a proper bipolar spindle. Although *Saccharomyces cerevisiae* and *Schizosaccharomyces pombe* SPBs are morphologically distinct from each other and from the human centrosome, over half of the components of both yeast SPBs have a human orthologue (Fig. 1 A). Furthermore, analyses of the SPB in both species have provided key insights into centrosome function in mammals, including the mechanism of microtubule formation by γ-TCs and evidence that centrosomes/SPBs are assembled in a stepwise manner from a central core structure in a highly regulated process involving multiple kinases (Kilmartin, 2014; Fu et al., 2015; Lin et al., 2015).

Extensive cytological, molecular, and genetic characterization of the *S. cerevisiae* SPB has led to robust models of its structure, duplication, and function (Jaspersen and Winey, 2004; Winey and Bloom, 2012; Lin et al., 2015). However, detailed molecular understanding of additional MTOCs in highly tractable genetic organisms is important to elucidate broad principles of assembly and regulation. The fission yeast SPB is an ideal choice based on descriptive analysis of SPB duplication from EM and a list of SPB components (Fig. 1 A). Although the fission yeast nuclear envelope (NE) remains intact during mitosis, the *S. pombe* SPB duplicates in the cytoplasm during G1 or S phase and is not inserted into the membrane until mitosis (McCully and Robinow, 1971; Ding et al., 1997; Uzawa et al., 2004; Höög et al., 2007). Thus, duplication is analogous to that of centrosomes, and the SPB is often found in a cytoplasmic NE invagination like that seen for centrosomes in some types of vertebrate cells (Robbins and Gonatas, 1964; Stafstrom and Staehelin, 1984; Baker et al., 1993; Tang and Marshall, 2012). Fission yeast SPBs are activated as MTOCs at approximately the same time they are inserted into the NE, where they remain until they are extruded back into the cytoplasm at telophase (Tanaka and Kanbe, 1986).

Components of the fission yeast SPB have been identified by a variety of approaches, and individual roles have been assigned based on analyses of loss-of-function mutant alleles and/or homology of the protein to orthologues in other organisms. Regional connections between several SPB subunits have been made; however, how individual submodules are connected

Correspondence to Sue L. Jaspersen: slj@stowers.org

Abbreviations used: DIC, differential interference contrast; EMM, Edinburgh minimal media; FRET, fluorescence resonance energy transfer; FWHM, full-width half-maximum; γ-TC, gamma tubulin complex; γ-TURC, gamma tubulin ring complex; γ-TUSC, gamma tubulin small complex; HU, hydroxyurea; INM, inner nuclear membrane; MTOC, microtubule-organizing center; NE, nuclear envelope; ONM, outer nuclear membrane; SIM, structured illumination microscopy; SIN, septation initiation network; SPA, single-particle analysis; SPB, spindle pole body.

The Rockefeller University Press
J. Cell Biol. Vol. 216 No. 8 2409–2424
https://doi.org/10.1083/jcb.201701041

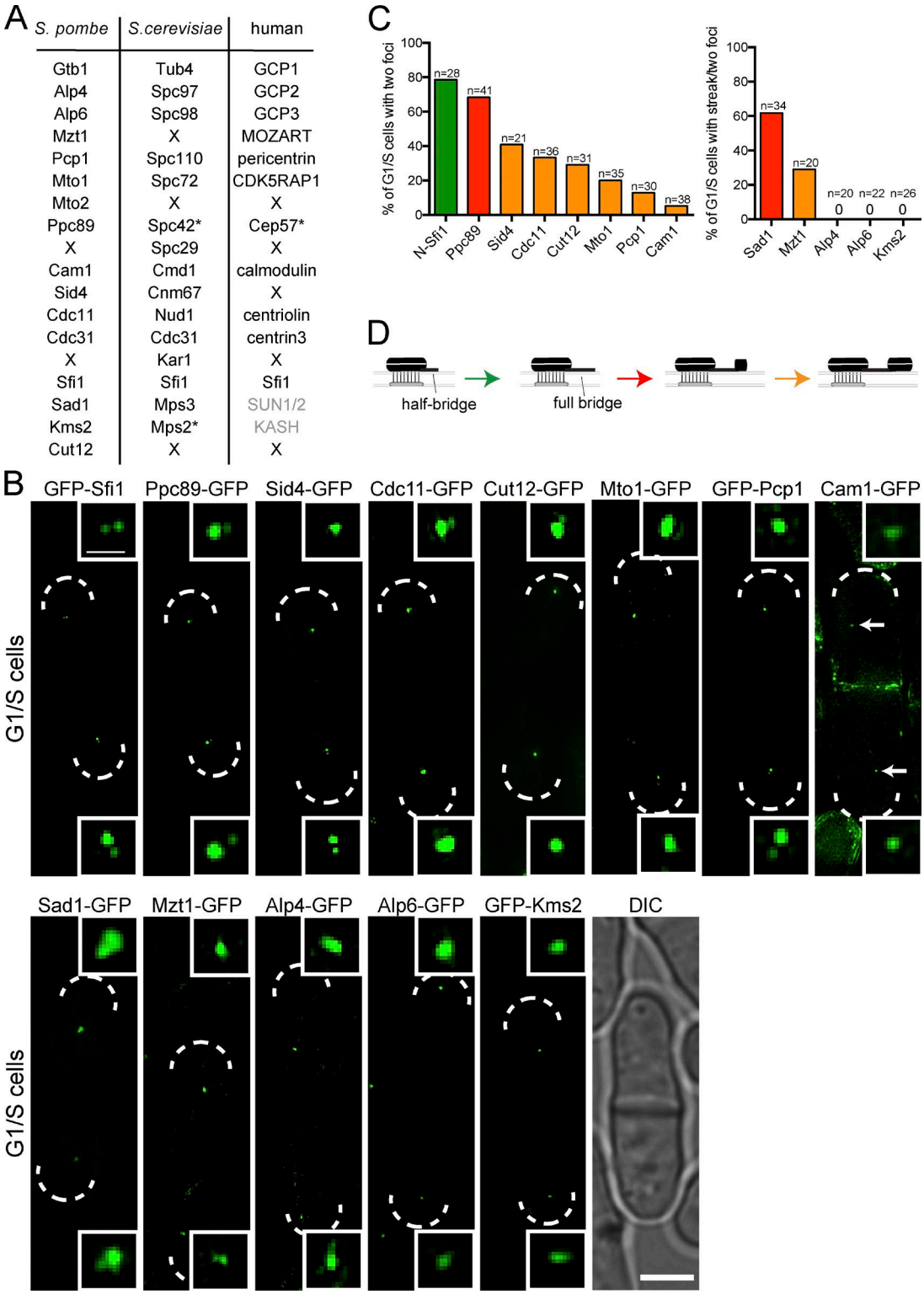

Figure 1. **Assembly of satellite SPB using SIM.** (A) List of SPB proteins in fission yeast used in this study and their known or predicted homologues in *S. cerevisiae* and *H. sapiens*. X, no homologue known; *, nonhomologous protein with similar function. Proteins in gray have not been reported to have roles in centrosome duplication. (B) G1/S cells were identified within asynchronous population of cells containing GFP-tagged core SPB components (top row) or membrane/bridge/γ-TC proteins (bottom row) based on a septum in the differential interference contrast (DIC) image, as shown in the last panel. The ends of the cells are shown by dashes. Two SPBs could be detected by SIM, one in each cell. Bar, 3 µm. Insets show a magnified region of the SPB. Arrows point to SPBs in Cam1-GFP. Bar, 0.5 µm. (C) Percentage of G1/S cells that contained two closely spaced foci (top). For membrane/bridge/γ-TC proteins, two foci or an extended GFP signal was detected (Fig. S1 C); both were quantitated as described in Materials and methods (bottom). The number of cells is shown. Protein localization fell into four classes: greater than 75% (green), 50–75% (red), 5–45% (orange), and 0% of cells with two foci, suggesting a temporal order of assembly during SPB duplication shown in D.

and how the fission yeast SPB assembles has never been comprehensively examined. For example, it is known that Sfi1 and Cdc31 are conserved components of the membrane-associated region of the SPB known as the half-bridge that is important for SPB duplication (Kilmartin, 2003; Paoletti et al., 2003; Lee et al., 2014; Bouhlel et al., 2015), but it is unknown how they interact with other SPB proteins to assemble the new SPB. Similarly, Ppc89 binds to Sid4, which is required to localize Cdc11 and septation initiation network (SIN) components to the SPB (Chang and Gould, 2000; Tomlin et al., 2002; Rosenberg et al., 2006). However, how the Ppc89–Sid4–Cdc11 SPB module interacts with γ-TC linkers Pcp1 and Mto1/Mto2 is poorly understood. Although microtubule nucleation by the γ-tubulin small (γ-TSC; composed of Gtb1, Alp4, and Alp6) or ring complexes (γ-TRC; composed of Gtb1, Alp4, Alp6, Gfh1, Mod21, and Alp16) has been studied extensively at other fission yeast MTOCs (Horio et al., 1991; Vardy and Toda, 2000; Flory et al., 2002; Fujita et al., 2002; Venkatram et al., 2004; Samejima et al., 2005; Anders et al., 2006), considerably less is known about microtubule formation at the SPB. Lastly, the molecular nature of how the SPB is tethered to the NE is unclear. Although the SUN domain–containing protein Sad1 localizes to the inner nuclear membrane (INM) region beneath the SPB constitutively (Hagan and Yanagida, 1995), the outer nuclear membrane (ONM) KASH domain–containing protein Kms2 is enriched at the SPB only in mitotic cells (Wälde and King, 2014). Thus, how Sad1 is connected to the cytoplasmic SPB during interphase if its linker is not present remains elusive.

To resolve these outstanding questions regarding *S. pombe* SPB structure and determine how the pole is duplicated during the cell cycle, we analyzed the distribution of 14 fission yeast SPB components throughout the cell cycle using structured illumination microscopy (SIM) alone and together with single-particle averaging (SPA; Burns et al., 2015). Our timeline of SPB assembly begins with bridge elongation via Sfi1 followed by deposition of Ppc89. We provide evidence that Ppc89, although not orthologous to Spc42 from budding yeast, plays a functionally similar role in SPB assembly. Our imaging-based approach to MTOC structure also allowed us to visualize proteins (Kms2, Cut12, and Mzt1) that are not present in budding yeast (Bridge et al., 1998; Tallada et al., 2009; Dhani et al., 2013; Masuda et al., 2013; Wälde and King, 2014; Masuda and Toda, 2016). We found striking similarities and differences between *S. cerevisiae* and *S. pombe* SPB in the organization of γ-TCs, and importantly, we could visualize intermediates in SPB insertion to enhance our understanding of MTOC function in higher eukaryotes.

Results

Creating a temporal hierarchy of *S. pombe* SPB duplication using SIM

The small size of the fission yeast SPB (180 nm in diameter, 90 nm in height; Ding et al., 1997) falls below the ∼200-nm resolution limit of conventional widefield and confocal microscopes. SIM provides a twofold increase in this resolution limit (Gustafsson et al., 2008). Therefore, to investigate how the SPB is duplicated and assembled in *S. pombe*, we used SIM with various GFP-tagged components of the fission yeast SPB. Strains containing GFP fusions grew at comparable rates to wild-type yeast and contained the same fraction of mitotic cells (Fig. S1 A). This includes N-terminally tagged GFP fusions that were expressed using the *nmt1* promoter (*41nmt1* for Kms2 and Pcp1 and *81nmt1* for Sfi1) at the native locus; under the conditions used for our experiments, GFP-fusion proteins expressed from this promoter were present at levels identical to or lower than those of endogenously expressed proteins (Fig. S1 B). Using SIM, we could detect one or two foci at the SPB in asynchronously growing log-phase cells (Fig. S2). Cam1-GFP also localized to sites of polarized growth such as the cell tip and septum, consistent with previous work (Moser et al., 1997). GFP-Cdc31 exhibited diffuse signal throughout the cell in addition to the SPB, likely because of its ectopic expression (Paoletti et al., 2003).

The appearance of a second closely spaced spot of GFP fluorescence at the SPB region by SIM is likely to be the new SPB, known as the satellite. To estimate when in the cell cycle each protein arrives at the new SPB, we divided cells into four categories based on cell morphology: G1/S phase (septated cells), early G2 (small <9.5 µm, recently divided cells), late G2 (elongated cells >11 µm with SPBs within 200 nm of each other), and mitotic cells (elongated cells with SPBs further than 200 nm apart; Fig. S2). A temporal hierarchy of component assembly emerged from this analysis, as illustrated in the percentage of G1/S cells with satellite GFP signal (Fig. 1, B and C, top).

Despite reduced signal compared with C-terminally tagged Sfi1 (Fig. S1 B), GFP-Sfi1 (N-Sfi1) had the highest percentage (79%) of G1/S cells with a satellite GFP signal, consistent with previous findings showing that Sfi1 is the initial protein to function in *S. pombe* SPB duplication (Lee et al., 2014; Bouhlel et al., 2015). Ppc89, a component of the SPB core, was apparent at the satellite of 68% in G1/S cells. The appearance of Ppc89 in a significantly higher fraction of G1/S cells compared with other core components (Cam1, Sid4, and Cdc11), linkers (Pcp1 and Mto1), and the SPB-activating protein Cut12 suggests Ppc89 is the first satellite component (Fig. 1, B and C). The observation that *ppc89+* depletion leads to loss of Sid4, Cdc11, and Pcp1 from the SPB is consistent with a role for Ppc89 early in assembly of the new SPB (Rosenberg et al., 2006). Although Ppc89 and *S. cerevisiae* Spc42 are not related at the amino acid sequence level, their early timing of assembly and role in recruitment of multiple SPB components suggests they are functionally equivalent (Fig. 1 A).

Multiple SPB components (Sad1, Mzt1, Alp4, Alp6, and Kms2) did not appear exclusively as one or two foci; extended streaks or lines were also observed in a fraction of cells, presumably because of distribution along the bridge or other SPB substructure linking the mother SPB and satellite (Fig. S1 C; see below). Given the likely contribution of expansion beyond the mother to SPB duplication, we included these streaks in our quantitation of G1/S foci if they extended at least 150 nm away from the SPB toward the satellite, a distance approximately equal to that of the extended bridge (see Fig. 2 D). Interestingly, Sad1 was observed as an extended streak or in two foci in 62% of G1/S phase cells (Fig. 1, B and C), suggesting that like Ppc89, it localizes to new SPB structures early in duplication. Extended streaks or two foci of Mzt1-GFP were observed in 28% of G1/S cells but were not seen for Alp4-GFP, Alp6-GFP, or GFP-Kms2 (Fig. 1, B and C). The accumulation of proteins like Alp4, Alp6, and Kms2 may be highly regulated or could require the formation of SPB substructures that are not present until later in the cell cycle.

Combining our results with previous data, we propose a general order of fission yeast SPB assembly that begins by

Sfi1-mediated bridge extension in late mitosis/G1, deposition of Ppc89 at the distal tip of the bridge early in G1, the buildup of other core proteins and linkers throughout G1 and S phase, and then finally addition of the γ-TC proteins in early G2 (Fig. 1 D). Analysis of cells containing the contractile ring component Rlc1-tdTomato provided further support for this scheme, because early septating G1/S cells contain a contractile ring and later septating G1/S cells lack it (Fig. S1 D; Wu et al., 2003). The early and late arrival of Sad1 and Kms2, respectively, is not understood, as they are thought to interact across the nuclear membrane (Wälde and King, 2014). Here, we further investigate the timing and mechanism of SPB assembly to further validate this model.

Sfi1 half-bridge extension initially favors the satellite SPB and is angled from the NE

Sfi1 is a long α-helical protein that localizes to centrosomes/SPBs in yeast, humans, and ciliates (Kilmartin, 2003; Rüthnick and Schiebel, 2016). In budding yeast, Sfi1 initiates elongation of the half-bridge, most likely via oligomerization of its C-terminal ends, which results in a new antiparallel array of Sfi1 with free N termini for construction of the new SPB (Kilmartin, 2003; Li et al., 2006; Burns et al., 2015; Seybold et al., 2015). Because previous studies in fission yeast were unable to localize Sfi1 by immuno-EM, we used SIM to study the structure of the Sfi1 and its binding partner, Cdc31, at the half-bridge.

C-terminally tagged Sfi1 (Sfi1-C) mostly appeared as a single focus throughout the cell cycle, like GFP-Cdc31 but unlike N-Sfi1 (Fig. 1, B and C; and Figs. 2 A and S2). To compare positional information of Sfi1 and Cdc31 during the cell cycle, we arrested cells in G1 by nitrogen starvation for 16 h, in S phase using 10 mM hydroxyurea (HU) for 4 h, or in late G2 using the *cdc25.22* mutant (3.5 h at 36°C; Fig. 2 B). Using previously developed computational methods, we aligned our dual-color SIM based on a fiducial marker located at the mother SPB and satellite (Ppc89-mCherry), a method known as SPA-SIM (Fig. 2 B). From these aligned images, the center of GFP-Sfi1, Sfi1-GFP, and GFP-Cdc31 fluorescence relative to Ppc89-mCherry was mapped and plotted: the x-axis represents the mother-satellite axis, whereas the y-axis represents the pole axis in our realignment scheme (Fig. 2 C). A table with the complete realignment parameters, including the full-width half-maximum (FWHM) values, is in Table S1.

Several notable features were observed based on this analysis. First, the C terminus of Sfi1 and Cdc31 did not colocalize with the core SPB, as previously predicted based on immuno-EM and fluorescence imaging (Paoletti et al., 2003; Bouhlel et al., 2015). Rather, both localize near the center of the 159 ± 2 nm elongated bridge (Fig. 2, B–D; and Table S1). Similar to budding yeast (Burns et al., 2015), Sfi1 filaments connecting to the satellite SPB are longer (∼1.25×) than filaments connecting to the mother SPB, particularly in S phase and late G2 (Fig. 2 D). In addition, the elongated bridge exhibits a kink in the negative direction of the pole axis, which is perpendicular to the NE, that increases during the cell cycle (Fig. 2 E). Bridge buildup away from the NE and reorientation of the SPBs as seen by EM are perhaps the simplest mechanisms to explain this phenomenon (Ding et al., 1997; Uzawa et al., 2004), but their importance for SPB duplication is unknown.

GFP-Sfi1 seemed equal or more intense on the distal region of the bridge compared with the proximal region in G1 and S phase (Fig. 2 B). To quantitate this difference, we analyzed cycling cells using cell morphology and SPB separation to determine cell cycle position because this alleviates concerns over aberrant SPB structures that may form during prolonged cell cycle arrests. Our data showing that GFP-Sfi1 fluorescence increases during the cell cycle are consistent with previous work (Lee et al., 2014; Bouhlel et al., 2015); however, our high-resolution SIM data show that accumulation occurs at both the mother and satellite, although Sfi1 levels are greater in the distal region of the extended bridge during duplication (Fig. 2 F), a finding that is highly reminiscent of Sfi1 distribution in budding yeast (Burns et al., 2015). Collectively, our SIM and SPA-SIM analysis of the fission yeast bridge shows that its extension occurs early in the cell cycle and likely requires oligomerization of Sfi1 C termini to form an antiparallel array with an N-terminal Sfi1 end near the satellite. Cdc31 is enriched in the central region of the bridge (Fig. 2 G).

Structure of the SPB core

After elongation of the bridge, Ppc89 was the first core SPB component to appear as two foci, followed by multiple other core proteins (Sid4, Cdc11, and Cam1), proteins that link the SPB to the γ-TC (Mto1 and Pcp1), and the SPB-activating protein Cut12. We were interested in examining the distribution of these components at the mother SPB and at the newly formed daughter SPB to understand SPB assembly. However, the lack of a comprehensive map of protein–protein interactions linking the entire SPB complex together, combined with immuno-EM on only a few SPB components, makes it difficult to determine protein position and orientation in the SPB relative to other SPB components. For example, is a given core factor more nuclear or more cytoplasmic than the C terminus of Ppc89?

To address this problem, we first performed SPA-SIM on cells containing Sad1-mCherry as the fiducial marker, because it is located at the INM, and all SPB components in interphase should be cytoplasmically shifted relative to it (Hagan and Yanagida, 1995). For each protein, we measured the distance from the center of GFP fluorescence to that of mCherry fluorescence, positioning each SPB component as shown in Fig. S3 (A–C). SPA-SIM of Cam1-GFP, Cdc11-GFP, Cut12-GFP, Mto1-GFP, GFP-Pcp1, Pcp1-GFP, and Sid4-GFP using Pcp89-mCherry as the fiducial marker showed that six of seven were present in two foci in S phase–arrested cells. In all cases, the more intense focus colocalized with the brighter spot of Ppc89-mCherry at the mother SPB, and the dimmer focus colocalized with the less intense spot of Ppc89-mCherry at the new SPB (Fig. 3 A). Because proteins localize to both the old and new pole during this period of cell division, we could investigate spatial relationships between components at both structures. Probability profiles show the average position of a GFP-tagged SPB component after alignment using Ppc89-mCherry (Fig. 3, B and C) and positional information from the Gaussian fits further refine the location at which the center of fluorescence was observed (Table S1). GFP-Pcp1 and Cut12-GFP are located at −40 and −38 nm on the pole axis at both the mother and the new pole, near the predicted position of the NE. This is consistent with the observation that they interact with the KASH-domain protein, Kms2, which localizes to the ONM region of the NE (Wälde and King, 2014). Cam1 binds to a region of the C terminus of Pcp1 in vitro (Flory et al., 2002), and it overlapped with Pcp1-GFP at the mother SPB (Fig. 3, B and C). Previous data suggest that the C termini of Ppc89 and Sid4 exhibit fluorescence res-

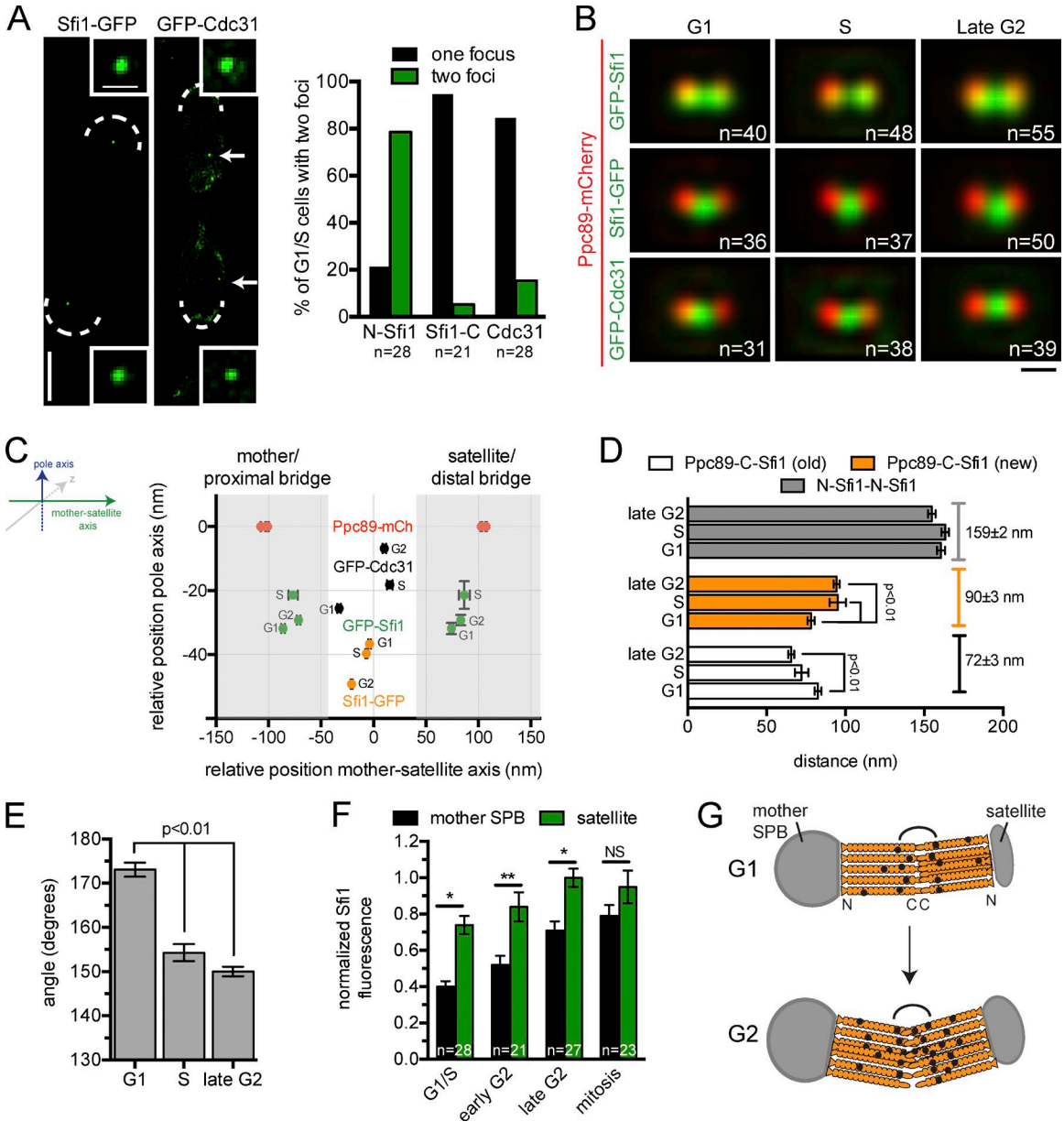

Figure 2. **Structure of the *S. pombe* bridge.** (A) G1/S cells containing GFP-Cdc31 or Sfi1-GFP were identified within the asynchronous population based on a septum in the DIC image, as in Fig 1 B. Arrows point to the SPBs in GFP-Cdc31. Bars: (main) 3 µm; (inset) 0.5 µm. The percentage of cells containing one or two foci two foci is shown. (B) SPA-SIM images of Ppc89-mCherry with GFP-Sfi1 (top), Sfi1-GFP (center), or GFP-Cdc31 (bottom). Cells were synchronized in G1 (nitrogen starvation for 16 h at 25°C), S (10 mM HU for 4 h at 25°C), and late G2 (*cdc25.22* mutant, 36°C for 3.5 h). The number of images used to create the projection is indicated (n). Bar, 200 nm. (C) Location of proteins derived from SPA-SIM in (B) were determined for both the pole and mother-satellite axes and plotted using the Ppc89-mCherry signal at the mother and new SPB as the zero reference position. Error bars represent SEM. n, as in B. The positions of the mother/bridge proximal region and satellite/bridge distal region were determined based on mean FWHM values of Ppc89-mCherry at the mother and satellite (Table S1). (D and E) Distance and angles were determined in three dimensions using GFP-Sfi1 foci and Ppc89-mCherry/Sfi1-GFP on the old and new Sfi1 filament that is proximal and distal to the mother SPB, respectively, from data in C. Error bars represent SEM. n, as in B. Indicated values are statistically significant based on Student's *t* test ($P < 0.01$). (F) Within an asynchronous population, the intensity of GFP-Sfi1 at the mother and satellite SPB was quantitated in the indicated number of individual images (n), and the mean level in each cell cycle stage (determined using DIC image) was calculated. For comparison purposes, values were normalized setting the highest observed value (satellite in late G2) to 1.0. Error bars represent SEM. n, as in B. P-values were determined using Student's *t* test, *, $P \leq 0.0001$; **, $P = 0.002$; NS, $P > 0.05$. (G) Schematic view of the elongated bridge showing the bend in Sfi1 (orange) that progresses during the cell cycle, the preferential association of Sfi1 to the satellite and the position of Cdc31 near the center of the bridge (black circles).

onance energy transfer (FRET; Rosenberg et al., 2006), which typically occurs over small distances. Thus, it is not surprising that the center of Sid4-GFP fluorescence was ~15 nm from the C terminus of Ppc89, whose center was less well positioned because of poorer resolution at longer red wavelengths. Although we were unable to perform SPA-SIM using N-terminally tagged Sid4 for technical reasons, we predict that the protein must extend in the cytoplasmic direction along the pole axis given that the N terminus of Sid4 interacts with the C terminus of Cdc11 in other assays (Krapp et al., 2001; Tomlin et al., 2002), which we find positioned at 25 nm. In the yeast two-hybrid system, Cdc11 and Mto1 interact (Samejima et al., 2010). Cdc11-GFP

and Mto1-GFP lie in the same region along the pole axis, but they are separated by 52 nm along the mother-satellite axis, likely because of migration of Mto1 onto the bridge (see Figs. 3, 4, and 5). The two-hybrid system could detect an interaction that occurs at a different point in the cell cycle or between regions of Cdc11 and/or Mto1 not represented by the GFP tag, which is represented in our maps.

A major gap in our global map arises from an incomplete understanding of how proteins near the NE, such as Pcp1, Cut12, and Cam1, are connected to more cytoplasmic components, such as Ppc89, Sid4, Cdc11 and Mto1. Both Ppc89 and Pcp1 are large proteins with coiled-coil domains (Flory et al., 2002; Rosenberg et al., 2006). In budding yeast, coiled-coil containing proteins frequently serve as structural scaffolds to join adjacent SPB layers (Kilmartin et al., 1993; Schaerer et al., 2001; Muller et al., 2005). To test if Ppc89 and Pcp1 perform similar roles in *S. pombe*, we analyzed the position of the N and C terminus of both Ppc89 and Pcp1 by SPA-SIM using Sad1-mCherry as the fiducial marker and by immuno-EM. If Ppc89 and/or Pcp1 connect adjacent regions of the SPB, we would anticipate finding the N terminus in one layer and the C terminus in a second. Consistent with this idea, the N terminus of Pcp1 was close to the NE in both the mother and new SPB, whereas the C terminus extended into the cytoplasm, reaching a region containing the N terminus of Ppc89. The C terminus of Ppc89 extended further toward the cytoplasm (Fig. 3, D–G; and Table S1). This strongly supports the possibility that Ppc89 and Pcp1 function as scaffolds to connect different layers of the fission yeast SPB. The proximity of the N terminus of Ppc89 and the C terminus of Pcp1 by SIM and EM suggests a direct physical interaction (Fig. 3 H), although we have failed to find evidence for this using FRET or other assays.

Assembly of the SPB core

To further refine our proposed assembly pathway and to characterize an early SPB duplication intermediate previously seen by EM (Uzawa et al., 2004), we performed SIM on nitrogen-starved cells, which results in an arrest with greater than 70% of cells in G1. The uniform arrest in these early G1 cells allowed us to approximate the timing of arrival of SPB core components at the new SPB by scoring the number of foci in individual SIM images: Ppc89-mCherry at the satellite SPB, but not SPB protein-GFP (2R:1G); both Ppc89-mCherry and SPB protein-GFP at the satellite SPB (2R:2G); or SPB protein-GFP at the satellite SPB, but not Ppc89-mCherry (1R:2G; Fig. 4 B). Virtually all (97%) G1-arrested cells had two foci of Ppc89-mCherry, one at the old mother SPB and one at the satellite, confirming our data from asynchronous cells that it is the first core SPB component to assemble at the satellite (Fig. 1, B and C; and Fig. S1 D). For other components, we found that 86% of Sid4, 80% of Pcp1, 72% of Cut12, 67% of Cdc11, and 60% of Cam1 cells contained two foci (Fig. 4 B). The fraction of cells is higher than we observed in asynchronous cells (Fig. 1 C), most likely because SPB size increases during the prolonged arrest, making SPB components easier to visualize (not depicted). The trend of this data with regard to gene order is consistent with known physical interactions (Krapp et al., 2001; Flory et al., 2002; Tomlin et al., 2002; Fong et al., 2010; Wälde and King, 2014), suggesting that assembly of Sid4 and Pcp1 occurs before that of interacting proteins like Cdc11, Cut12, and Cam1.

Although two foci of Cam1-GFP, Cdc11-GFP, Cut12-GFP, GFP-Pcp1, and Sid4-GFP were observed in some arrested G1 and S phase cells (Fig. 1, B and C; and Figs. 3 A, 4 A, and S1 D), the relative level of protein at the new SPB compared with the mother SPB varied considerably, with Cdc11-GFP present at the lowest levels. One possible explanation is that the SPB is assembled from a nuclear core involving Ppc89 in a stepwise process and that proteins such as Cdc11 can only incorporate after other proteins are added. An alternative possibility is that addition of certain SPB components is highly regulated and is coordinated with cell cycle progression. In this scenario, Cdc11 levels might be low because cells have not yet reached the time when it is maximally incorporated into the SPB. To explore these ideas, we examined the intensity of GFP-tagged SPB components in an asynchronous population of wild-type cells, binning cells into four cell cycle categories based on cell morphology and SPB separation, as described above. Using wild-type cells rather than arrested cells or mutants alleviated concerns over aberrant protein accumulation and abnormal SPB duplication intermediates that may not occur in a normal cell cycle. Because total SPB fluorescence intensity depends on the relative stoichiometry of components, which is unknown, we normalized values by setting the highest cell cycle category for each protein to 1.0. Ppc89 is not only the first protein to arrive, but it is also the first to fully mature at the new SPB, reaching maximum levels in late G2 (Fig. 4 C). Levels of other core/linker proteins, including Cam1-GFP, Cut12-GFP, GFP-Pcp1, and Sid4-GFP, gradually increase on the new SPB during G2 phase to at least 0.67-fold of mitotic levels, which are the highest we observed (Fig. 4 C). In contrast, Cdc11-GFP only reached 0.51- ± 0.05-fold of mitotic levels in late G2. The fact that other core/linker SPB components have begun to accumulate in late G2 whereas Cdc11 has not lends support to a model in which Cdc11 recruitment to the new SPB is highly regulated, possibly as part of symmetry breaking in SIN (Feoktistova et al., 2012).

Unlike other core/linker proteins, Mto1-GFP did not form two foci in G1 or S phase cells; it colocalized with either the mother SPB or with the bridge. In budding yeast, the Mto1 orthologue, Spc72, relocalizes to the bridge during SPB duplication and mating (Pereira et al., 1999). However, the Spc72 receptor on the bridge, Kar1, is not conserved (Fig. 1 A), and no cytoplasmic microtubules nucleating from the fission bridge have been reported in EM studies (McCully and Robinow, 1971; Tanaka and Kanbe, 1986; Ding et al., 1993, 1997; Uzawa et al., 2004; Höög et al., 2007). Examination of asynchronously growing cells containing Mto1-GFP and Mto1-GFP/Ppc89-mCherry and GFP-Pcp1/Ppc89mCherry cells in G1, S, and late G2 phases using SPA-SIM showed that Mto1-GFP accumulation on the new SPB did not occur until later in G2 phase (Figs. S2 and S3 D). Previous work suggested that Mto1 localization to the SPB is Cdc11 and Sid4 independent during much of interphase (Samejima et al., 2010). Our data showing that Mto1 is present in a single focus at the SPB during this same period, combined with localization to the bridge (a region of the SPB lacking Cdc11 and Sid4), suggest a novel interphase recruitment pathway. Mto1 recruitment to the SPB during late G2 and mitosis uses a second platform involving Cdc11.

The γ-TC proteins Alp4 and Alp6 localize near the NE and span the bridge

The γ-TC is recruited to the SPB via the linkers, Mto1/Mto2 and Pcp1, as well as by Mzt1, a small protein that binds directly to the γ-TC (Venkatram et al., 2004, 2005; Janson et al., 2005; Samejima et al., 2005, 2008, 2010; Fong et al., 2010; Dhani et

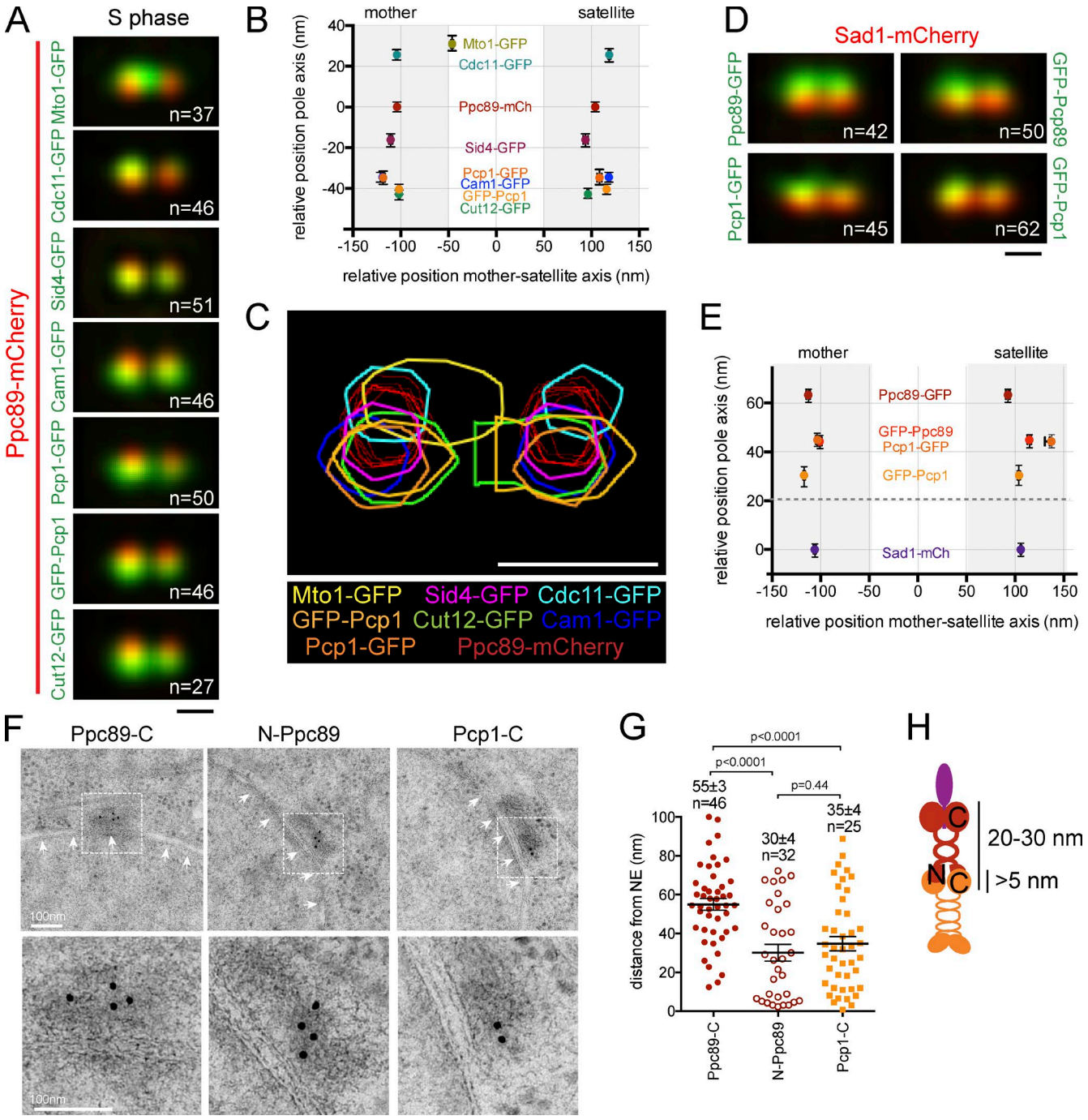

Figure 3. **Localization of SPB core and linker components during S phase.** (A) SPA-SIM images of Ppc89-mCherry and indicated core SPB protein-GFP synchronized in S phase cells. Number of images, n. Bar, 200 nm. (B) Location of core SPB proteins derived from SPA-SIM in A. The maximum intensity of the Cam1-GFP, Cdc11-GFP, Cut12-GFP, Mto1-GFP, GFP-Pcp1, Pcp1-GFP, and Sid4-GFP distributions were determined for both the pole and mother-satellite axes and plotted using the Ppc89-mCherry signal at the mother and new SPB as the zero reference position. Error bars represent SEM. n, as in A. Based on the FWHM values of Ppc89-GFP at the mother (129 nm, −168 to −39 nm) and satellite (120 nm; 44 to 164 nm; Table S1), the bridge was divided into proximal/mother and distal/satellite regions. (C) Contour map showing the distribution of the fluorescent intensity of the core SPB proteins (colored as indicated) of images from A. Ppc89-mCherry for each sample is shown in red. Bar, 200 nm. (D) SPA-SIM images of S phase–arrested Sad1-mCherry containing N- or C-terminal GFP-tagged Ppc89 or Pcp1. Number of images, n. Bar, 200 nm. (E) Positional location of Ppc89 and Pcp1 derived from SPA-SIM images in (D). The maximum intensity of fits of Ppc89-GFP, GFP-Ppc89, Pcp1-GFP, and GFP-Pcp1 distributions were determined for both axes and plotted using the Sad1-mCherry signal at the mother and the satellite as the zero reference position. Error bars represent SEM. n, as in D. FWHM values are listed in Table S1, and the bridge was divided into proximal/mother and distal/satellite regions, using positional information from B. The approximate positions of the NE based on EM data are also shown. (F) Immuno-EM of Ppc89-GFP, GFP-Ppc89, and Pcp1-GFP. Arrows indicate the NE. A magnified region containing gold particles at the SPB is shown below. Bar, 100 nm. (G) Quantification of the indicated number of gold particles from at least 20 EM images of interphase cells. The distance of individual gold particles was measured in ImageJ at an angle of 90° from the NE. Error bars show the mean distance and SEM. P-values were calculated using the Student's *t* test. (H) Schematic showing the orientation of Ppc89 N and C termini (red) along with the approximate distance based on SIM data from the C terminus of Pcp1 (Table S1). The projections of GFP-Pcp1/Ppc89-mCherry and Ppc89-GFP/Sad1-mCherry in A and D are also shown in Fig. S3 (D and A, respectively).

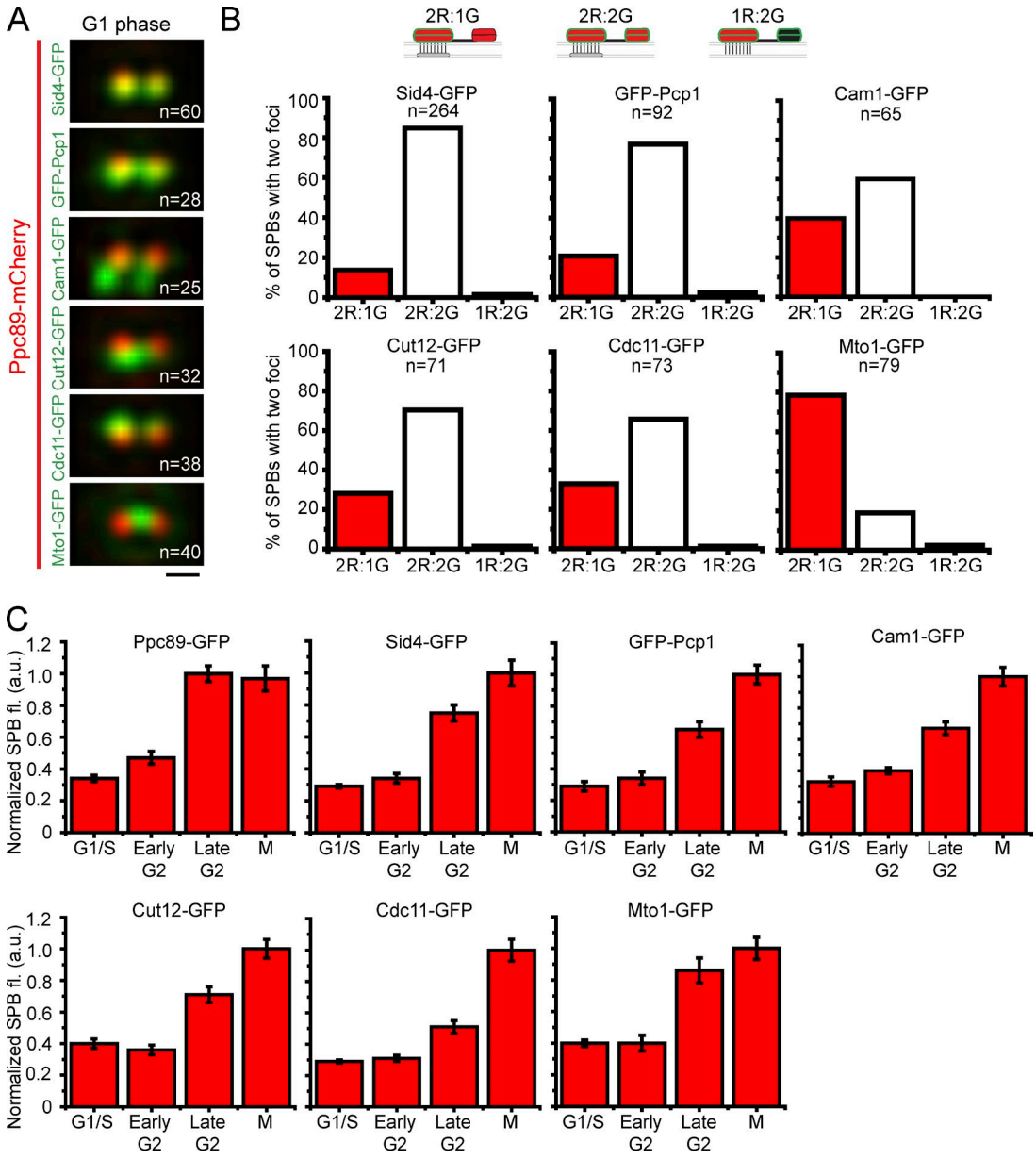

Figure 4. **Assembly of core and linker components at the SPB.** (A) SPA-SIM of G1-arrested Ppc89-mCherry cells containing the indicated core SPB GFP-fusion. The number of images (n) used to create the projection is shown. Bar, 200 nm. (B) Individual images from A were analyzed to determine the number of SPBs that contained two red foci of Ppc89-mCherry and one or two foci of GFP at the mother and satellite (denoted 2R:1G and 2R:2G, respectively), as shown in the schematic. A fraction of cells that contained two GFP foci and a single focus of Ppc89-mCherry (1R:2G) were also observed. (C) Asynchronously growing cells at 25°C containing the indicated GFP-tagged SPB component were imaged by SIM, and the intensity of GFP at the satellite was determined. For comparison purposes, values for each protein were then normalized setting the highest observed value to 1.0. Cell cycle position was determined by cell morphology from an identical DIC image. Error bars represent SEM; $n \geq 20$ cells for each cell cycle quantified. The projection of Mto1-GFP/Ppc89-mCherry is also shown in Fig. S3 D.

al., 2013; Masuda et al., 2013). Based on the localization of Mto1 to the bridge, we were interested in the distribution of γ-TC subunits, Gtb1, Alp4, and Alp6. We were unable to create viable strains of *gtb1+* fused with GFP at either terminus, so we focused on the localization of Alp4-GFP and Alp6-GFP. In asynchronously growing G1/S phase cells, we never detected either protein at the new SPB using SIM (Fig. 1 C), but two spots or a streak of fluorescence was visible by early G2 phase (Figs. S1 C and S2). The broad band of Alp4-GFP and Alp6-GFP that migrated into the bridge region is somewhat reminiscent of Mto1-GFP, although Mto1-GFP was more restricted in its distribution (compare Fig. 3 A to Fig. 5 A). SPA-SIM of Alp4-GFP/Ppc89-mCherry and Alp6-GFP/Ppc89-mCherry cells arrested in G1, S, or late G2 phase confirmed that most Alp4-GFP and Alp6-GFP fluorescence is located between the mother SPB and satellite marked by Ppc89-mCherry, similar to the distribution of Mzt1-GFP (Fig. 5 A). In late G2, a second population of Alp4-GFP, Alp6-GFP, and Mzt1-GFP appears opposite the large population that is present since G1. As we discuss in the next section, we believe the large focus is Alp4, Alp6, and Mzt1 accumulating on the side of the SPB adjacent to the NE, whereas the population in late G2 is Alp4, Alp6, and Mzt1 on the cytoplasmic face.

Previous immuno-EM using anti-Gtb1 antibodies suggested that a large pool of Gtb1 accumulated inside the nu-

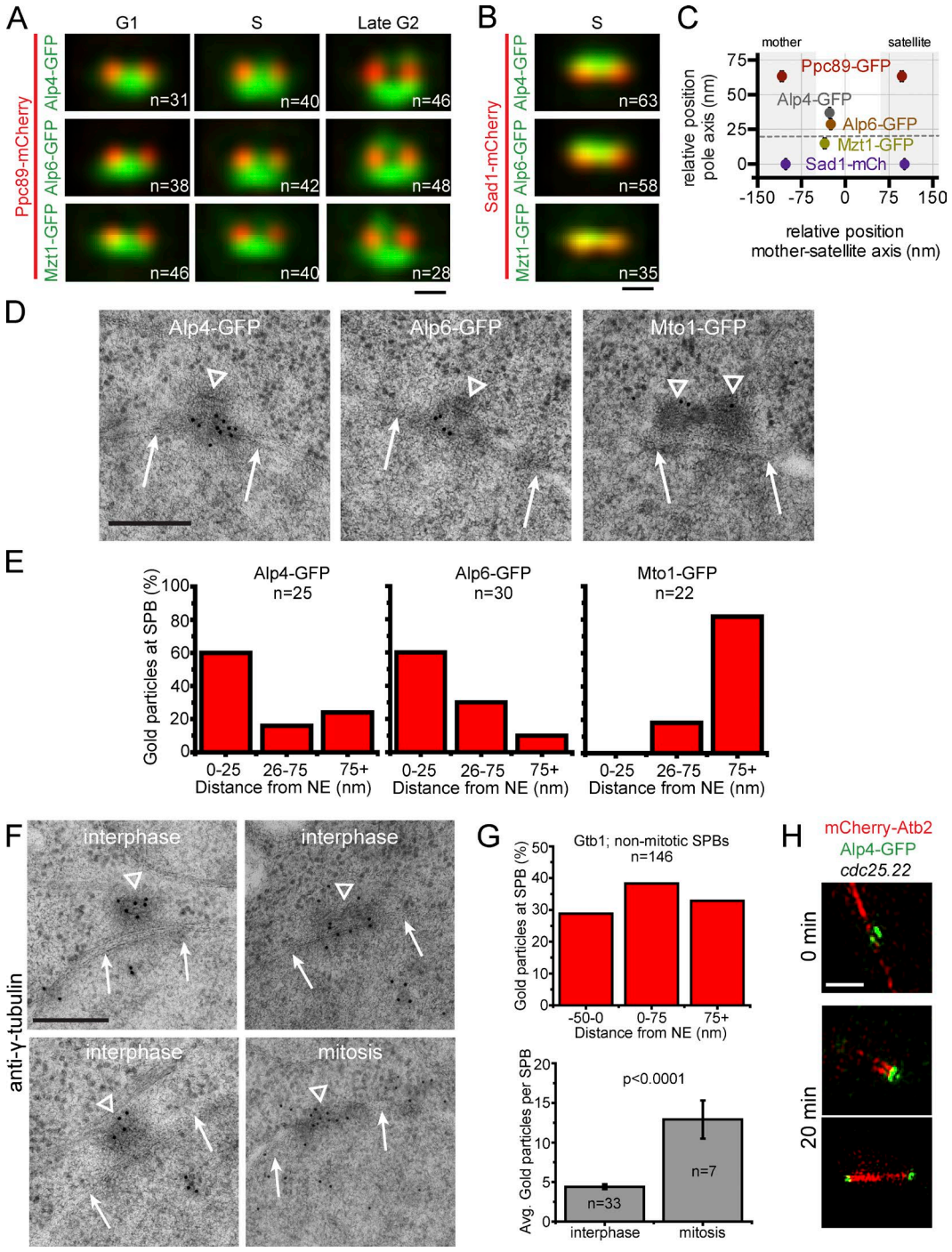

Figure 5. **γ-Tubulin complex components, Alp4 and Alp6, localize near the NE between duplicated SPBs.** (A) SPA-SIM images of Ppc89-mCherry with Alp4-GFP (top), Alp6-GFP (middle), or Mzt1-GFP (bottom) arrested in G1, S, or late G2. The number of images used to create the projection is indicated (n). Bar, 200 nm. (B) SPA-SIM of Sad1-mCherry with Alp4-GFP (top), Alp6-GFP (middle), or Mzt1-GFP (bottom) from the indicated number of S phase–arrested cells. Bar, 200 nm. (C) The maximum intensity of the Alp4-GFP, Alp6-GFP, or Mzt1-GFP distributions were determined from images in B in the pole and mother-satellite axes and plotted using the Sad1-mCherry signal at the mother and the satellite as the zero reference position. Ppc89-GFP is also shown, with FWHM values used to delineate proximal/mother and distal/satellite regions. Error bars represent SEM. n, as in B. Complete FWHM values for all data points are listed in Table S1. The approximate position of the NE is shown by the dashed line. (D) Anti-GFP immuno-EM of interphase cells containing Alp4-GFP, Alp6-GFP, and Mto1-GFP. Arrows indicate the NE, and arrowheads indicate the SPB. Bar, 200 nm. (E) The distance of individual gold particles was measured in ImageJ at an angle of 90° from the NE. The number (n) of images is shown. (F) Immuno-EM was also performed with polyclonal antibodies that recognize the amino acids 38–53 in γ-tubulin. Three interphase cells and one mitotic cell are shown. Bar, 100 nm. (G) Gold particles were quantitated as in E, with negative and positive numbers representing the nuclear and cytoplasmic sides of the NE. Also shown is the number of gold particles detected at the SPB in interphase and mitotic cells. Error bars show SEM. P-value was calculated using Student's *t* test. (H) *cdc25.22* cells containing mCherry-Atb2 and Alp4-GFP were synchronized in late G2 for 4 h at 36°C and then released into mitosis for 20 min by incubation at 25°C and imaged by SIM. Cytoplasmic microtubules were seen perpendicular to the SPB before release (top), whereas parallel microtubules from a single SPB (middle) and in a bipolar spindle (bottom) are seen after release. Bar, 1 µm. The projection of Alp4-GFP/Sad1-mCherry is also shown in Fig. S3 A.

cleus adjacent to the SPB in interphase (Ding et al., 1997). The purpose of this stockpile is unknown given the lack of nuclear microtubules throughout interphase in *S. pombe* (Tanaka and Kanbe, 1986; Hagan and Hyams, 1988; Höög et al., 2007). To determine if other components of the γ-TC or its regulators are also located here, we positioned Alp4, Alp6, Mzt1, and Ppc89 in S phase–arrested cells using SPA-SIM and Sad1-mCherry as the fiducial marker. Although Alp4-GFP and Alp6-GFP are more proximal to Sad1-mCherry than Ppc89-GFP, both are located over 30 nm away along the pole axis, suggesting that the proteins are on the cytoplasmic face of the NE (Fig. 3 E; Fig. 5, B and C; and Table S1). At ∼15 nm, the shift of Mzt1-GFP relative to Sad1-mCherry is the smallest; however, based on its binding to the N terminus of Alp6 (Dhani et al., 2013), it is also likely cytoplasmic during S phase (Fig. 5, B and C).

To confirm the cytoplasmic localization of the γ-TC during interphase, we performed immuno-EM on asynchronously growing Alp4-GFP and Alp6-GFP cells using anti–GFP antibodies followed by secondary antibodies conjugated to colloidal gold. Most of the signal for Alp4-GFP and Alp6-GFP (∼60%) was found in the cytoplasm within 25 nm of the NE, whereas a small subset (23% for Alp4, 10% for Alp6) was found further than 75 nm from the membrane (Fig. 5, D and E). This distant cytoplasmic population likely corresponds to the small population of Alp4 and Alp6 that we see in late G2. For comparison, 82% of gold particles used to detect Mto1-GFP were ≥75 nm away from the nuclear membrane and often appeared in the region between duplicated SPBs, similar to Mto1-GFP distribution in our SIM images (Fig. 5, D and E). Immuno-EM using an affinity-purified monoclonal antibody that cross-reacts with a 16-amino-acid region in the N terminus of Gtb1 also showed an enrichment for gold particles at SPBs, which increased as cells entered mitosis (Fig. 5, F and G). These data suggest that a significant fraction of γ-tubulin is cytoplasmic, like Alp4 and Alp6; however, we did observe gold particles on the nuclear side of the NE in some cells, so we cannot entirely exclude the possibility of a small nuclear pool of γ-tubulin during interphase.

Our observation of Mzt1, Alp4, Alp6, and γ-tubulin at the SPB raised an interesting question: are these complexes competent for microtubule formation? Nuclear microtubules are formed from the large dash of Alp4-GFP proximal to the NE as cells enter mitosis (Fig. 5 H, middle) and progress through metaphase into anaphase (Fig. 5 H, bottom). SPB-associated microtubules were not detected at other times during cell division; instead, interphase microtubules running perpendicular to the SPB were observed (Fig. 5 H, top), suggesting that the nuclear membrane prevents γ-TC activation or serves as a physical barrier to microtubule elongation during most of the cell cycle.

Timing of Sad1 and Kms2 localization to the new SPB

Perhaps one of our most surprising results was that Sad1 localized to the bridge and satellite considerably earlier than its presumed binding partner, Kms2 (Fig. 1, B and C). To confirm this result was not caused by slow growth of the GFP-Kms2 strain, we analyzed G1, S, and late G2 phase–arrested cells with Ppc89-mCherry as the fiducial marker using SPA-SIM. Both proteins appear broadly distributed across the region between the two SPBs in merged images; however, GFP-Kms2 is restricted to the bridge region near the mother SPB until late G2, whereas Sad1-GFP appears at both poles in early G1 (Fig. 6 A). Quantitation of individual images from G1-arrested cells confirmed this observation, showing that 84.8% of G1 SPBs had both Ppc89 (Fig. 6 B, red) and Sad1 (green) at the satellite compared with 17.9% of SPBs with Kms2 signal at the satellite. Use of a stronger or weaker *nmt1* promoter did not affect the fraction of G1 or early G2 cells containing two foci of Kms2 (Fig. S1 E), consistent with the idea that its accumulation at the SPB is up-regulated before mitosis (Wälde and King, 2014).

The early arrival of Sad1 at the new SPB suggested a role during the early stages of SPB assembly, possibly in bridge formation, like Mps3 function at the budding yeast SPB (Jaspersen et al., 2002, 2006). If Sad1 is required early in SPB duplication, then we would anticipate that either the bridge would not elongate and/or early components of the new SPB would not be deposited in a temperature sensitive mutant at 36°C, events we can now directly assay using SIM via GFP-Sfi1 and Ppc89-GFP, respectively, in *sad1.1* mutants. At 36°C, the mutant displayed defects in SPB inheritance, which included cells with zero, one, or two SPBs (Fig. 6 C). Despite this issue, two foci of GFP-Sfi1 were observed in 76.9% of mutant cells at 25°C and 62.2% at 36°C, a difference that was not significant ($P = 0.11$). Ppc89-GFP localization to the new SPB was also observed in 63.9% of mutant cells at 25°C and 61.3% at 36°C, which also was not significant ($P = 0.83$; Fig. 6 D) as anticipated based on findings of Bouhlel et al. (2015). These data suggest that although Sad1 is present at the satellite region early, Sad1 function is not required for key steps of early duplication such as bridge elongation and deposition of the first core component.

After a prolonged G2 arrest at 36°C in *cdc25.22* mutants, we found images in which Sad1-GFP shifted from underneath the duplicated side-by-side SPBs to a full or partial ring surrounding Ppc89-mCherry. We could increase the fraction of cells containing a Sad1-GFP ring by synchronously releasing these cells into mitosis by lowering the temperature to 25°C for 10 to 20 min before imaging. Sad1-GFP shifted from the side-by-side orientation (Fig. 6 E, left, side-on view) to a ring-like distribution around one Ppc89-mCherry locus (Fig. 6 E, middle, top-down view) to a larger ring distribution that appears to surround both SPBs (Fig. 6 E, right, top-down view). We cannot examine how Sad1-GFP is redistributed in real-time because we cannot resolve the ring by confocal imaging and SIM is not compatible with long-term time-lapse imaging. However, three lines of evidence lead us to believe that these ring-like structures are related to insertion of the fission yeast SPB into the NE. First, mutation of *sad1+* results in SPB insertion errors (Hagan and Yanagida, 1995; Fernández-Álvarez et al., 2016). Second, the timing of Sad1 redistribution correlates with that of SPB insertion into the NE, occurring just after release from *cdc25.22*. Lastly, when we examined the distribution of Alp4-GFP/Sad1-mCherry in *cdc25.22*-arrested cells, a significant fraction of Alp4-GFP moved ∼40 nm in the pole axis toward the NE (in comparison to S phase localization) so that it is now "below" the Sad1 (Fig. 5, B and C; Fig. 6, F and G; and Table S1). Because these cells do not nucleate microtubules, it is unclear if an actual hole in the membrane has formed or if Alp4-GFP is present in a NE fenestra like that described by EM (Ding et al., 1997; Uzawa et al., 2004). Our data suggest that Sad1 is present at the SPB early to set up structures that will trigger SPB insertion before the cell even enters mitosis.

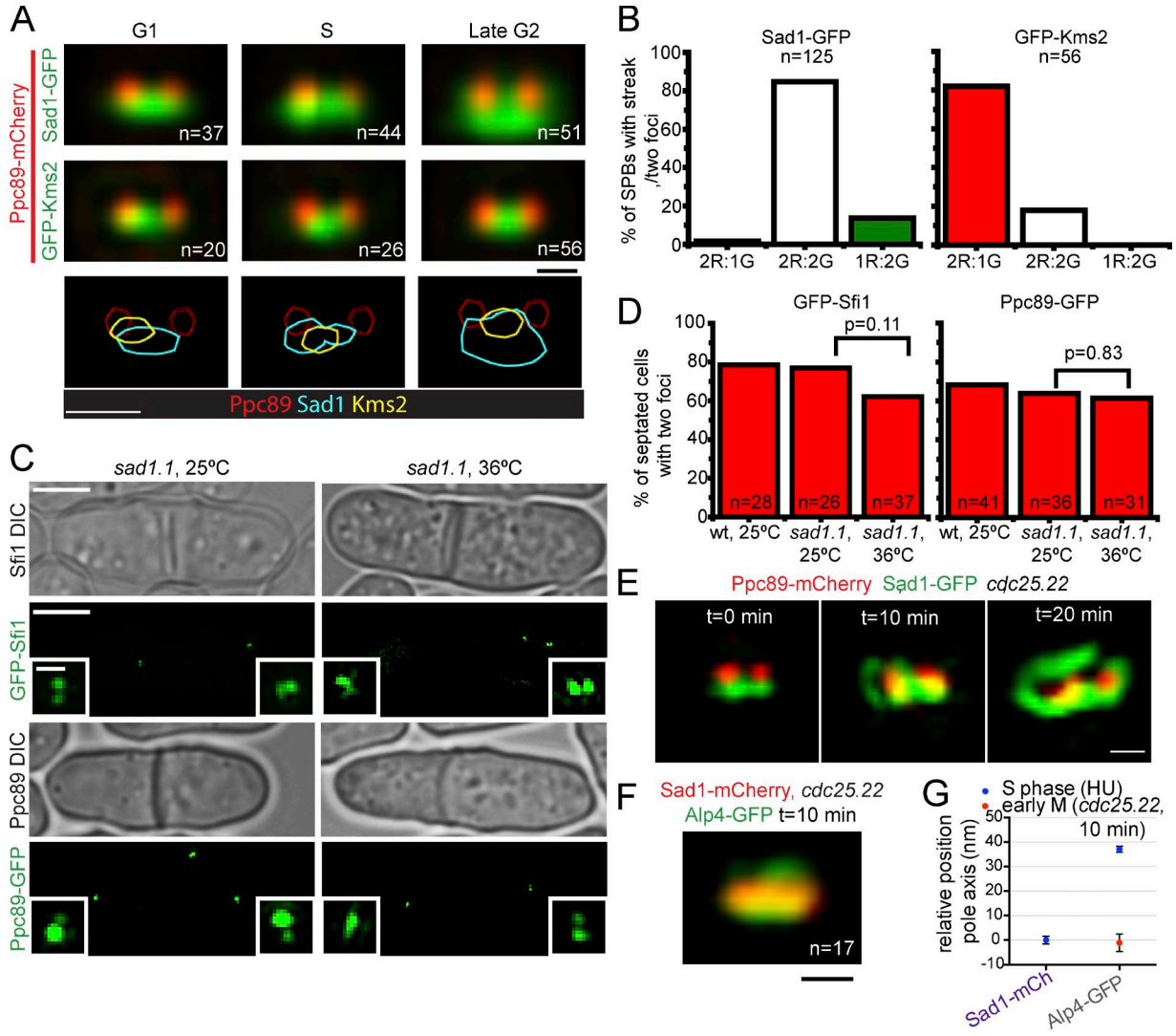

Figure 6. **Sad1 and Kms2 localization to the SPB by SIM.** (A) SPA-SIM images of Ppc89-mCherry with Sad1-GFP (top) or GFP-Kms2 (middle) from G1-, S-, or late G2–arrested cells. The number of images used to create the projection is indicated (n). Bar, 200 nm. Bottom contour maps show the distribution of the fluorescent intensity Sad1 (cyan) and Kms2 (yellow) from the images above. Ppc89-mCherry for each sample is shown in red. Bar, 200 nm. (B) Ppc89-mCherry cells containing Sad1-GFP or GFP-Kms2 were arrested in G1 phase by nitrogen starvation for 16 h at 25°C then analyzed by SIM to determine the number (n) of SPBs that contained two red foci of Ppc89-mCherry and one or two foci of GFP at the mother and satellite (denoted 2R:1G and 2R:2G, respectively). Cells that contained two GFP foci and a single focus of Ppc89-mCherry (1R:2G) were also observed. (C) *sad1.1* cells containing either GFP-Sfi1 (top) or Ppc89-GFP (bottom) were grown at 25°C, and then cultures were divided, with one kept at 25°C for 4 h (left) and the other culture shifted to 36°C for 4 h (right). Cells were examined by SIM, and example images of cells with SPBs are shown. Bars, 3 µm. Insets show a magnified region containing the SPB. Bar, 500 nm. (D) Percentage of septated cells from (C) that had either GFP-Sfi1 or Ppc89-GFP signal at the satellite in the *sad1.1* background. Wild-type (wt) cells were included to ensure that *sad1.1* cells at 25°C were not already compromised. Total number of septated cells examined is listed. P-values were determined using Student's *t* test; none were statistically significant. (E) *cdc25.22* cells containing Ppc89-mCherry and Sad1-GFP were grown overnight at 25°C, arrested in late G2 by growth at 36°C for 3.5 h, and then released into mitosis by shifting back to 25°C for 0, 10, and 20 min. Example images from each time point are shown to illustrate how Sad1-GFP localizes beneath the SPBs in late G2 (left; side-on view) and then localizes to a region around a single SPB (middle; top-down view) and finally around both SPBs (right; top-down view). Bar, 200 nm. (F) SPA-SIM of *cdc25.22* Sad1-mCherry Alp4-GFP early mitotic cells that were released from *cdc25.22* arrest for 10 min. Alp4-GFP signal is below Sad1-mCherry signal in the pole-axis. Bar, 200 nm. (G) Position of maximum intensity of Sad1-mCherry and Alp4-GFP along the pole-axis (y) in S (from Fig 5, B and C) and cells in F with Sad1-mCherry as the zero reference position. Error bars represent SEM (see Table S1). n, as in Figs. 5 B and 6 F.

Discussion

High-resolution analysis of the fission yeast SPB allowed us to clarify at a molecular level the timing of its duplication during cell division and the mechanism of SPB assembly. Analysis of Sfi1 distribution through the cell cycle showed that it accumulates in two waves: it is recruited to the SPB quickly in mitosis/G1/S (before cytokinesis finishes) and then slowly accumulates to even higher levels at the SPB throughout G2 (Lee et al., 2014). Because we can resolve the mother SPB and satellite, we show that the initial burst of Sfi1 is primarily caused by the accumulation of protein distal to the mother SPB to form the extended half-bridge (Fig. 7 A). However, as the cell cycle continues, this preference is lost and Sfi1 is added to both proximal and distal regions, possibly forming stacked sheets, as observed by EM (Paoletti et al., 2003; Höög et al., 2013). In wild-type *S. cerevisiae*, the Sfi1 filament is thought to exist in a monolayer caused by tethering by Kar1 (Seybold et al., 2015). Kms2 is an

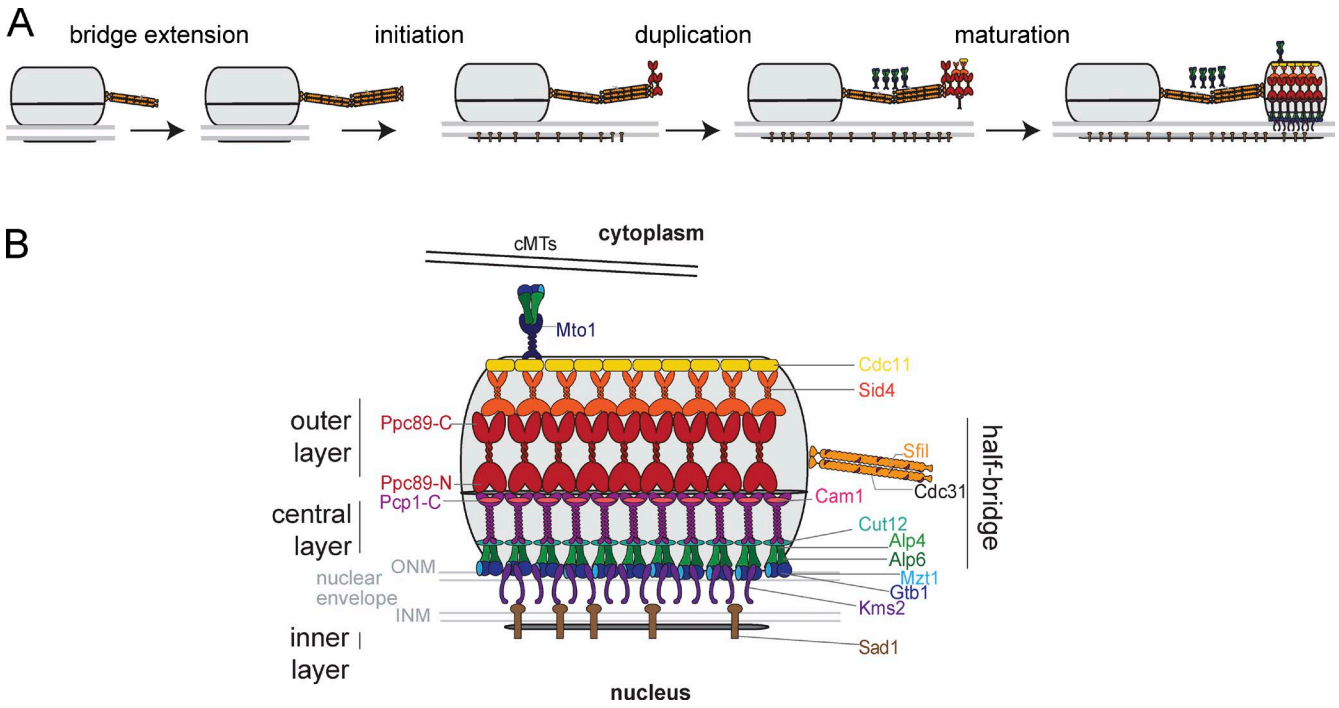

Figure 7. **Model for *S. pombe* SPB duplication and maturation during the cell cycle.** Schematic of SPB duplication (A) based on data described throughout, with key molecules indicated based on B.

ONM *S. pombe* SPB component, but at least two lines of evidence suggest that Kms2 does not perform a Kar1-like function: (1) Kms2 is not distributed along the bridge during most of the cell cycle, and (2) loss of Kms2 function results in SPB insertion failure rather than an inability to nucleate a new structure, the phenotype of *kar1* mutants in budding yeast (Vallen et al., 1992, 1994; Wälde and King, 2014).

Based on its early recruitment to the satellite SPB and its requirement for SPB localization of multiple SPB components, we propose that Ppc89 functions as a platform for assembly of a new SPB (Fig. 7 A). The C terminus of Ppc89 has previously been shown to interact with Sid4 (Rosenberg et al., 2006), and our SPA-SIM data show that this end of Ppc89 extends away from the NE to function in assembly of an outer module that includes Sid4, Cdc11, and Mto1. The N terminus of Ppc89 is located near the C terminus of Pcp1, which would facilitate assembly of a central module, which contains Cam1 in addition to Pcp1 (Fig. 7 B). The idea that Pcp89 connects SPB submodules makes it functionally analogous to Spc42 in budding yeast. Like Ppc89, Spc42 is also the first component recruited to the bridge, and its C and N terminus interact with orthologues of Sid4 (Cnm67) and Pcp1 (Spc110; Muller et al., 2005; Burns et al., 2015). Although SPA-SIM and immuno-EM data suggest that fluorophores on the N terminus of Ppc89 and the C terminus of Pcp1 are in close proximity, we have been unable to observe FRET between these two proteins. Although this may be explained by steric issues, this binding has not been detected by other approaches, possibly indicating an unknown protein might bridge Ppc89 and Pcp1. In budding yeast, Spc29 is found at the interface between the N terminus of Spc42 and the C terminus of Spc110 (Elliott et al., 1999; Muller et al., 2005). The idea that Ppc89 and Spc42 are functionally equivalent raises the possibility that similar factors are involved more globally at MTOCs. It is tempting to speculate that the Cep57 module within the centriole of centrosomes might play an analogous role (Fig. 1 A). Recent work suggests it facilitates interactions between the centriole core and the pericentriolar material, playing roles in its stability and microtubule nucleation capability (Wu et al., 2012; Lukinavičius et al., 2013).

The idea that Ppc89, like Spc42, serves as a scaffold for SPB assembly poses interesting new questions as to how its levels and interactions are regulated to ensure that SPB duplication and size are coupled with the cell cycle. Ppc89 levels at the SPB did not significantly increase from late G2 into mitosis. This contrasts to other core and linker proteins, including Sid4, Pcp1, Cut12, Mto1, and Cam1, which accumulate gradually at the new SPB throughout G2, then exhibit a burst of SPB accumulation as cells enter mitosis (Fig. 7 A). The fact that the Ppc89 scaffold accumulates early suggests that ample Ppc89 sites exist for Sid4 and Pcp1 during S and G2 phases. Presumably the Ppc89 sites remain vacant until SPB maturation in mitosis stimulates Sid4, Pcp1, and other proteins to accumulate at the SPB. Based on studies of Pcp1 and Cut12 (Grallert et al., 2013; Wälde and King, 2014), maturation/accumulation of SPB components is linked to mitotic regulation and commitment to mitotic division.

Cdc11 is thought to recruit Mto1 to the mitotic SPB (Samejima et al., 2010). The lag in Cdc11 assembly until the onset of mitosis suggests that its assembly, and possibly that of Mto1-recruitment and microtubule nucleation, is highly regulated. However, our results point to a secondary Cdc11-independent pathway for Mto1 recruitment because a significant fraction of cells contained two Mto1 foci and only a single Cdc11 focus. Our ability to visualize the γ-TC proteins Alp4 and Alp6 and their regulator, Mzt1, at the SPB during interphase also suggests that the activity of the γ-TC is highly regulated. Although previous work suggested this might occur through sequestration of γ-tubulin within the nucleus during interphase (Ding et al.,

1997), our immuno-EM data suggest a significant fraction of γ-tubulin exhibits a cytoplasmic distribution, similar to Alp4 and Alp6. Thus, an important direction for future work is to understand why γ-TC activity/microtubule nucleation efficiency in interphase is low at the SPB compared with mitotic cells.

Sad1 and Kms2 are thought to interact in the luminal space between INM and ONM via their SUN and KASH domains to form a LINC complex (Wälde and King, 2014). The early and late arrival of Sad1 and Kms2, respectively, raises an important question: how does Sad1 at the INM spread from the mother SPB to the satellite without Kms2? This, combined with questions discussed above as to how Sfi1 and Mto1 are tethered to the bridge, perhaps point to the idea that additional membrane components of the SPB have yet to be identified. The finding that Sad1 spreads onto the bridge and satellite early parallels the localization of Mps3 in budding yeast (Burns et al., 2015) and suggests that, like *S. cerevisiae*, membrane-related structures are assembled during duplication even though NE fenestration does not occur until later. As cells entered mitosis, we observed that Sad1 formed a ring around one SPB that then enlarged to surround both poles. Based on the timing of ring assembly, we believe that these Sad1-containing structures modify the NE to enable the SPB to "drop in" to the membrane. Sad1 could facilitate insertion through a variety of mechanisms, such as activation of Cut12, recruitment of structural proteins that shape, bend, and remodel the membrane and/or recruitment of Kms2. Recent work suggested that binding of the LINCs complex to centromeres within the nucleus is crucial for SPB insertion, although the mechanism of how centromeric DNA bound to Sad1-Kms2 results in modification of the NE at the pole is currently unknown (Fernández-Álvarez et al., 2016). However, the interaction of Sad1 with centromeres could provide a mechanism that allows it to expand at the INM during interphase.

In conclusion, we have developed the first molecular model of the fission yeast SPB using a combination of imaging-based methods. This approach allowed us to understand how components of the SPB assembled during duplication to form a structure that can nucleate microtubules both inside and outside the nucleus. Drawing on knowledge from the budding yeast SPB, we could determine conserved principles of assembly that are likely to exist at all MTOCs as well as predict functions of proteins that share little sequence identity. Broadly speaking, this type of comparative approach will be useful in analysis of protein complexes and organelles in a wide range of organisms.

Materials and methods

Yeast strains and strain construction

S. pombe strains used in this study are listed in Table S2, including many GFP-tagged strains obtained from various laboratories: *pcp1* (J.R. McIntosh, University of Colorado, Boulder, CO), *sid4* (J. Cooper, National Institutes of Health, Center for Cancer Research, Bethesda, MD), *alp4* and *alp6* (K. Sawin, Wellcome Trust Centre for Cell Biology, Edinburgh, Scotland, UK), N-terminally tagged *sfi1* and *cdc31* (J.-Q. Wu, The Ohio State University, Columbus, OH), *kms2* (M. King, Yale University School of Medicine, New Haven, CT), *cdc11*, *pcp1*, and N-terminally tagged *ppc89* (K. Gould, Vanderbilt University, Nashville, TN), and *cam1* (T. Davis, University of Washington, Seattle, WA). Other fusions to GFP and/or mCherry were created using PCR-based methods that target the endogenous locus as described previously (Bähler et al., 1998). These tags were introduced directly or through crosses into prototrophic wild-type, *mCherry-atb2*, and *sad1-mCherry* strains, gifts from P. Baumann (Stowers Institute for Medical Research, Kansas City, MO), J.R. McIntosh, and D. Kovar (University of Chicago, Chicago, IL), respectively.

Cell cycle growth and microscopy

Growth of GFP-tagged strains was analyzed in rich yeast-extract media (YE5S) for ∼24 h at 25°C, with back dilutions to ensure they remained logarithmic. Equivalent numbers of cells were concentrated, serially diluted, and spotted onto YE5S plates at 25°C, 30°C, and 36°C. Cells from these same cultures were also fixed with 70% ethanol for 15 min before DAPI staining (final concentration: 2 µg/ml) to determine the percentage of cells with two DNA foci.

To analyze asynchronously growing yeast, cells were grown in YE5S for ∼24 h at 25°C, with back dilutions to ensure they remained logarithmic. Cells were then transferred to Edinburgh minimal media with amino acid supplements (EMM5S) for 4 h at 25°C before collection for microscopy. Cell cycle position in these cells was determined using cell size, morphology, and structure as follows: G1 cells contained a visible septum, early G2 cells had completed cell splitting and were end-on or overlapping with a length between 7 and 9.5 µm, late G2 cells were between 11 and 14 µm and had SPBs closer than 200 nm, and mitotic cells lacked a septum and had SPBs greater than 200 nm apart.

Nitrogen starvation was used to synchronize prototrophic yeast cells in G1 using the following strategy. After ∼24 h in YE5S at 25°C, cells were transferred to EMM5S for ∼8 h at 25°C. Cells were then washed twice with EMM media that lacked nitrogen (EMM-N_2) and contained only 1/10 the normal supplements (uracil, leucine, histidine, lysine, and adenine; slightly modified from Su et al., 1996). Subsequently, strains were grown for ∼16 h in EMM-N_2 media at 25°C before imaging. FACS analysis of the procedure showed that 70% of cells were in G1 phase (1N). Because fluorophores faded over time in nitrogen-starved cells, images were taken within 2 h of fixation.

Cells were synchronized in S phase with HU. After growth for ∼24 h in YE5S at 25°C, samples were washed in EMM5S and then transferred into EMM5S at 25°C for 1 h before the addition of 10 mM HU for 4 h at 25°C before imaging.

Synchronization in late G2 used *cdc25.22*. Cells were grown for ∼24 h in YE5S at 25°C, transferred to EMM5S for 1 h at 25°C, and then shifted to 36°C for 3.5 h before imaging. To release cells from the arrest, cultures were transferred back to 25°C for 10 or 20 min.

To prepare cells for imaging, cells were fixed with 4% paraformaldehyde (Ted Pella) in 100 mM sucrose for 20 min, pelleted by a brief centrifugation at 3,000 rpm, and then washed twice in PBS, pH 7.4. After the last wash, cells were resuspended in a small volume of PBS and then visualized by SIM. Fixation was important to prevent movement during SIM.

SIM imaging and SPA-SIM

SIM images were obtained with an Applied Precision OMX Blaze V4 (GE Healthcare) using a 60× 1.42 NA Olympus Plan Apo oil objective and two PCO Edge sCMOS cameras (one camera for each channel). All SIM microscopy was performed at 22–23°C. For the two-color GFP/mCherry experiments, a 405/488/561/640 dichroic was used with 504- to 552-nm and 590- to 628-nm emission filters for GFP and mCherry, respectively. Images were taken using a 488-nm laser (for GFP) or a 561-nm laser (for mCherry), with alternating excitation. SIM reconstruction was done with Softworx (Applied Precision Ltd.), with a Wiener filter of 0.001. SIM images shown in the publication were maximum projections over relevant z slices, scaled 4 × 4 with bilinear interpolation using ImageJ (National Institutes of Health).

SPA-SIM analysis was performed with custom written macros and plugins in ImageJ. All plugins and source code are available at

http://research.stowers.org/imagejplugins/. Individual spots of mother and satellite SPBs were fitted to two 3D Gaussian functions and realigned along the axis between these functions for further analysis using [jay_sim_fitting_macro_multicolor_profile.ijm]. Spot selection was performed in a semiautomated fashion with manual identification and selection of mother and satellite SPBs. A secondary protein (either Ppc89- or Sad1-mCherry) was used as a fiduciary marker to determine position of the GFP-labeled protein, so that all positions of the SPB proteins were compared with a single origin point. For both fiducial proteins, the higher intensity spot was assigned as the mother. After alignment, images were averaged and scaled as described previously (Burns et al., 2015), using [merge_all_stacks_jru_v1.ijm] then [stack_statistics_jru_v2.ijm]. Orientation of images along the pole axis was based on Sad1-mCherry relative positioning and the assumption that it is the most nuclear SPB component throughout interphase (see Fig. S3, A–C).

Contour maps were generated by thresholding each spot in each channel at 75% of its maximum intensity and outlining the resulting mask. Mother and daughter spots were contoured separately and, as a result, were limited to their respective sides of the image. In some cases, this results in the truncation of the contour at the midpoint along the satellite axis.

Image analysis and quantification

For measuring fluorescence intensities of the SPBs, the summed relevant z-sections were used. A circular region of interest was used with a 6-pixel diameter to measure the fluorescence intensity. Background was measured by taking the mean of three regions of interest fluorescence intensities taken in the cell, but not at the SPB. To determine whether a satellite SPB was present, after background correction in a maximum intensity projection, any fluorescent spot that was within 250 nm of the bright mother SPB and at least 15% of the mother SPB fluorescence intensity was counted as a satellite. Although the 15% threshold could underestimate the fraction of cells containing a satellite, it was used to prevent SIM reconstruction artifacts from being included in the data. For proteins that had a distribution that was a line instead of two dots (i.e., Alp4, Alp6, Mzt1, Sad1, and Kms2), a "satellite" SPB was counted when the line extended 150 nm away from the peak of the mother SPB fluorescence.

EM

Asynchronous, log-phase cells were high-pressure frozen in a Leica EM ICE (Leica Biosystems) high-pressure freezer, freeze-substituted in 0.2% uranyl acetate in acetone, processed for immuno-EM, and embedded in Lowicryl HM20 as described previously (Giddings et al., 2001). Sections were cut on a Leica UC6 ultramicrotome at 50 nm and labeled with anti–GFP antibody (a gift from M. Rout, Rockefeller University, New York, NY) and 12 nm Colloidal Gold-AffiniPure Goat Anti-Rabbit (Jackson ImmunoResearch Laboratories, Inc.). The anti–γ-tubulin antibody (ab11316; Abcam) was used with 12 nm Colloidal Gold-AffiniPure Goat Anti-Mouse (Jackson ImmunoResearch Laboratories, Inc.). Imaging was conducted using an FEI Technai BioTwin electron microscope.

Data

Original data underlying this paper can be downloaded from the Stowers Original Data Repository at http://www.stowers.org/pubs/LIBPB-1163.

Online supplemental material

Fig. S1 shows GFP-tagged SPB components, Fig. S2 shows localization to *S. pombe* SPB by SIM throughout cell division, and Fig. S3 shows positioning of SPB components along the pole axis using Sad1 and localization of Mto1 to the SPB. Table S1 shows probability distribution fit parameters and Table S2 lists yeast strains used in this study.

Acknowledgments

We thank Ken Sawin, Kathy Gould, Julie Cooper, Megan King, Peter Baumann, David Kovar, Iain Hagan, Dick McInstosh, Susan Forsburg, and Mike Rout for strains, plasmids, antibodies, and advice. We are grateful to the Stowers Institute's Microscopy Center and the Jaspersen laboratory for helpful discussions; to Melainia McClain, who helped with EM; and to Sarah Zanders, Brian Slaughter, Tina Sing, Christine Smoyer, Roxie Burger, and Sarah Smith for comments on the manuscript. We also thank Lynn Stoltz for helping make reagents, Ann Cavanaugh for assistance with the model, and Veronica Cloud for insightful discussion throughout the entire project.

Research reported in this publication was supported by the Stowers Institute for Medical Research and the National Institute of General Medical Sciences of the National Institutes of Health under award number R01GM121443 (to S.L. Jaspersen).

The authors declare no competing financial interests.

Author contributions: A.J. Bestul and S.L. Jaspersen conceived the experiments. A.J. Bestul constructed strains and performed arrests. A.J. Bestul and Z. Yu performed SIM. J.R. Unruh developed tools for image analysis. A.J. Bestul analyzed data, prepared figures, and wrote the paper with assistance from S.L. Jaspersen and input from all the authors.

Submitted: 5 January 2017
Revised: 17 April 2017
Accepted: 10 May 2017

References

Anders, A., P.C. Lourenço, and K.E. Sawin. 2006. Noncore components of the fission yeast gamma-tubulin complex. *Mol. Biol. Cell.* 17:5075–5093. http://dx.doi.org/10.1091/mbc.E05-11-1009

Bähler, J., J.Q. Wu, M.S. Longtine, N.G. Shah, A. McKenzie III, A.B. Steever, A. Wach, P. Philippsen, and J.R. Pringle. 1998. Heterologous modules for efficient and versatile PCR-based gene targeting in *Schizosaccharomyces pombe*. *Yeast.* 14:943–951. http://dx.doi.org/10.1002/(SICI)1097-0061(199807)14:10<943::AID-YEA292>3.0.CO;2-Y

Baker, J., W.E. Theurkauf, and G. Schubiger. 1993. Dynamic changes in microtubule configuration correlate with nuclear migration in the preblastoderm *Drosophila* embryo. *J. Cell Biol.* 122:113–121. http://dx.doi.org/10.1083/jcb.122.1.113

Bouhlel, I.B., M. Ohta, A. Mayeux, N. Bordes, F. Dingli, J. Boulanger, G. Velve Casquillas, D. Loew, P.T. Tran, M. Sato, and A. Paoletti. 2015. Cell cycle control of spindle pole body duplication and splitting by Sfi1 and Cdc31 in fission yeast. *J. Cell Sci.* 128:1481–1493. http://dx.doi.org/10.1242/jcs.159657

Bridge, A.J., M. Morphew, R. Bartlett, and I.M. Hagan. 1998. The fission yeast SPB component Cut12 links bipolar spindle formation to mitotic control. *Genes Dev.* 12:927–942. http://dx.doi.org/10.1101/gad.12.7.927

Burns, S., J.S. Avena, J.R. Unruh, Z. Yu, S.E. Smith, B.D. Slaughter, M. Winey, and S.L. Jaspersen. 2015. Structured illumination with particle averaging reveals novel roles for yeast centrosome components during duplication. *eLife.* 4:e08586. http://dx.doi.org/10.7554/eLife.08586

Chang, L., and K.L. Gould. 2000. Sid4p is required to localize components of the septation initiation pathway to the spindle pole body in fission yeast. *Proc. Natl. Acad. Sci. USA.* 97:5249–5254. http://dx.doi.org/10.1073/pnas.97.10.5249

Dhani, D.K., B.T. Goult, G.M. George, D.T. Rogerson, D.A. Bitton, C.J. Miller, J.W. Schwabe, and K. Tanaka. 2013. Mzt1/Tam4, a fission yeast MOZ ART1 homologue, is an essential component of the γ-tubulin complex and directly interacts with GCP3(Alp6). *Mol. Biol. Cell.* 24:3337–3349. http://dx.doi.org/10.1091/mbc.E13-05-0253

Ding, R., K.L. McDonald, and J.R. McIntosh. 1993. Three-dimensional reconstruction and analysis of mitotic spindles from the yeast, Schizosaccharomyces pombe. *J. Cell Biol.* 120:141–151. http://dx.doi.org/10.1083/jcb.120.1.141

Ding, R., R.R. West, D.M. Morphew, B.R. Oakley, and J.R. McIntosh. 1997. The spindle pole body of *Schizosaccharomyces pombe* enters and leaves the nuclear envelope as the cell cycle proceeds. *Mol. Biol. Cell.* 8:1461–1479. http://dx.doi.org/10.1091/mbc.8.8.1461

Elliott, S., M. Knop, G. Schlenstedt, and E. Schiebel. 1999. Spc29p is a component of the Spc110p subcomplex and is essential for spindle pole body duplication. *Proc. Natl. Acad. Sci. USA.* 96:6205–6210. http://dx.doi.org/10.1073/pnas.96.11.6205

Feoktistova, A., J. Morrell-Falvey, J.S. Chen, N.S. Singh, M.K. Balasubramanian, and K.L. Gould. 2012. The fission yeast septation initiation network (SIN) kinase, Sid2, is required for SIN asymmetry and regulates the SIN scaffold, Cdc11. *Mol. Biol. Cell.* 23:1636–1645. http://dx.doi.org/10.1091/mbc.E11-09-0792

Fernández-Álvarez, A., C. Bez, E.T. O'Toole, M. Morphew, and J.P. Cooper. 2016. Mitotic nuclear envelope breakdown and spindle nucleation are controlled by interphase contacts between centromeres and the nuclear envelope. *Dev. Cell.* 39:544–559. http://dx.doi.org/10.1016/j.devcel.2016.10.021

Flory, M.R., M. Morphew, J.D. Joseph, A.R. Means, and T.N. Davis. 2002. Pcp1p, an Spc110p-related calmodulin target at the centrosome of the fission yeast *Schizosaccharomyces pombe*. *Cell Growth Differ.* 13:47–58.

Fong, C.S., M. Sato, and T. Toda. 2010. Fission yeast Pcp1 links polo kinase-mediated mitotic entry to gamma-tubulin-dependent spindle formation. *EMBO J.* 29:120–130. http://dx.doi.org/10.1038/emboj.2009.331

Fu, J., I.M. Hagan, and D.M. Glover. 2015. The centrosome and its duplication cycle. *Cold Spring Harb. Perspect. Biol.* 7:a015800. http://dx.doi.org/10.1101/cshperspect.a015800

Fujita, A., L. Vardy, M.A. Garcia, and T. Toda. 2002. A fourth component of the fission yeast gamma-tubulin complex, Alp16, is required for cytoplasmic microtubule integrity and becomes indispensable when gamma-tubulin function is compromised. *Mol. Biol. Cell.* 13:2360–2373. http://dx.doi.org/10.1091/mbc.02-01-0603

Giddings, T.H. Jr., E.T. O'Toole, M. Morphew, D.N. Mastronarde, J.R. McIntosh, and M. Winey. 2001. Using rapid freeze and freeze-substitution for the preparation of yeast cells for electron microscopy and three-dimensional analysis. *Methods Cell Biol.* 67:27–42. http://dx.doi.org/10.1016/S0091-679X(01)67003-1

Grallert, A., K.Y. Chan, M.L. Alonso-Nuñez, M. Madrid, A. Biswas, I. Alvarez-Tabarés, Y. Connolly, K. Tanaka, A. Robertson, J.M. Ortiz, et al. 2013. Removal of centrosomal PP1 by NIMA kinase unlocks the MPF feedback loop to promote mitotic commitment in S. pombe. *Curr. Biol.* 23:213–222. http://dx.doi.org/10.1016/j.cub.2012.12.039

Gustafsson, M.G., L. Shao, P.M. Carlton, C.J. Wang, I.N. Golubovskaya, W.Z. Cande, D.A. Agard, and J.W. Sedat. 2008. Three-dimensional resolution doubling in wide-field fluorescence microscopy by structured illumination. *Biophys. J.* 94:4957–4970. http://dx.doi.org/10.1529/biophysj.107.120345

Hagan, I.M., and J.S. Hyams. 1988. The use of cell division cycle mutants to investigate the control of microtubule distribution in the fission yeast Schizosaccharomyces pombe. *J. Cell Sci.* 89:343–357.

Hagan, I., and M. Yanagida. 1995. The product of the spindle formation gene sad1+ associates with the fission yeast spindle pole body and is essential for viability. *J. Cell Biol.* 129:1033–1047. http://dx.doi.org/10.1083/jcb.129.4.1033

Höög, J.L., C. Schwartz, A.T. Noon, E.T. O'Toole, D.N. Mastronarde, J.R. McIntosh, and C. Antony. 2007. Organization of interphase microtubules in fission yeast analyzed by electron tomography. *Dev. Cell.* 12:349–361. http://dx.doi.org/10.1016/j.devcel.2007.01.020

Höög, J.L., S.M. Huisman, D. Brunner, and C. Antony. 2013. Electron tomography reveals novel microtubule lattice and microtubule organizing centre defects in +TIP mutants. *PLoS One.* 8:e61698. http://dx.doi.org/10.1371/journal.pone.0061698

Horio, T., S. Uzawa, M.K. Jung, B.R. Oakley, K. Tanaka, and M. Yanagida. 1991. The fission yeast gamma-tubulin is essential for mitosis and is localized at microtubule organizing centers. *J. Cell Sci.* 99:693–700.

Janson, M.E., T.G. Setty, A. Paoletti, and P.T. Tran. 2005. Efficient formation of bipolar microtubule bundles requires microtubule-bound gamma-tubulin complexes. *J. Cell Biol.* 169:297–308. http://dx.doi.org/10.1083/jcb.200410119

Jaspersen, S.L., and M. Winey. 2004. The budding yeast spindle pole body: Structure, duplication, and function. *Annu. Rev. Cell Dev. Biol.* 20:1–28. http://dx.doi.org/10.1146/annurev.cellbio.20.022003.114106

Jaspersen, S.L., T.H. Giddings Jr., and M. Winey. 2002. Mps3p is a novel component of the yeast spindle pole body that interacts with the yeast centrin homologue Cdc31p. *J. Cell Biol.* 159:945–956. http://dx.doi.org/10.1083/jcb.200208169

Jaspersen, S.L., A.E. Martin, G. Glazko, T.H. Giddings Jr., G. Morgan, A. Mushegian, and M. Winey. 2006. The Sad1-UNC-84 homology domain in Mps3 interacts with Mps2 to connect the spindle pole body with the nuclear envelope. *J. Cell Biol.* 174:665–675. http://dx.doi.org/10.1083/jcb.200601062

Kilmartin, J.V. 2003. Sfi1p has conserved centrin-binding sites and an essential function in budding yeast spindle pole body duplication. *J. Cell Biol.* 162:1211–1221. http://dx.doi.org/10.1083/jcb.200307064

Kilmartin, J.V. 2014. Lessons from yeast: The spindle pole body and the centrosome. *Philos. Trans. R. Soc. Lond. B Biol. Sci.* 369:1650. http://dx.doi.org/10.1098/rstb.2013.0456

Kilmartin, J.V., S.L. Dyos, D. Kershaw, and J.T. Finch. 1993. A spacer protein in the *Saccharomyces cerevisiae* spindle poly body whose transcript is cell cycle-regulated. *J. Cell Biol.* 123:1175–1184. http://dx.doi.org/10.1083/jcb.123.5.1175

Kollman, J.M., A. Merdes, L. Mourey, and D.A. Agard. 2011. Microtubule nucleation by γ-tubulin complexes. *Nat. Rev. Mol. Cell Biol.* 12:709–721. http://dx.doi.org/10.1038/nrm3209

Krapp, A., S. Schmidt, E. Cano, and V. Simanis. 2001. S. pombe cdc11p, together with sid4p, provides an anchor for septation initiation network proteins on the spindle pole body. *Curr. Biol.* 11:1559–1568. http://dx.doi.org/10.1016/S0960-9822(01)00478-X

Lee, I.J., N. Wang, W. Hu, K. Schott, J. Bähler, T.H. Giddings Jr., J.R. Pringle, L.L. Du, and J.Q. Wu. 2014. Regulation of spindle pole body assembly and cytokinesis by the centrin-binding protein Sfi1 in fission yeast. *Mol. Biol. Cell.* 25:2735–2749. http://dx.doi.org/10.1091/mbc.E13-11-0699

Li, S., A.M. Sandercock, P. Conduit, C.V. Robinson, R.L. Williams, and J.V. Kilmartin. 2006. Structural role of Sfi1p-centrin filaments in budding yeast spindle pole body duplication. *J. Cell Biol.* 173:867–877. http://dx.doi.org/10.1083/jcb.200603153

Lin, T.C., A. Neuner, and E. Schiebel. 2015. Targeting of γ-tubulin complexes to microtubule organizing centers: Conservation and divergence. *Trends Cell Biol.* 25:296–307. http://dx.doi.org/10.1016/j.tcb.2014.12.002

Lukinavičius, G., D. Lavogina, M. Orpinell, K. Umezawa, L. Reymond, N. Garin, P. Gönczy, and K. Johnsson. 2013. Selective chemical crosslinking reveals a Cep57-Cep63-Cep152 centrosomal complex. *Curr. Biol.* 23:265–270. http://dx.doi.org/10.1016/j.cub.2012.12.030

Masuda, H., and T. Toda. 2016. Synergistic role of fission yeast Alp16GCP6 and Mzt1MOZART1 in γ-tubulin complex recruitment to mitotic spindle pole bodies and spindle assembly. *Mol. Biol. Cell.* 27:1753–1763. http://dx.doi.org/10.1091/mbc.E15-08-0577

Masuda, H., R. Mori, M. Yukawa, and T. Toda. 2013. Fission yeast MOZART1/Mzt1 is an essential γ-tubulin complex component required for complex recruitment to the microtubule organizing center, but not its assembly. *Mol. Biol. Cell.* 24:2894–2906. http://dx.doi.org/10.1091/mbc.E13-05-0235

McCully, E.K., and C.F. Robinow. 1971. Mitosis in the fission yeast *Schizosaccharomyces pombe*: A comparative study with light and electron microscopy. *J. Cell Sci.* 9:475–507.

Moser, M.J., M.R. Flory, and T.N. Davis. 1997. Calmodulin localizes to the spindle pole body of *Schizosaccharomyces pombe* and performs an essential function in chromosome segregation. *J. Cell Sci.* 110:1805–1812.

Muller, E.G., B.E. Snydsman, I. Novik, D.W. Hailey, D.R. Gestaut, C.A. Niemann, E.T. O'Toole, T.H. Giddings Jr., B.A. Sundin, and T.N. Davis. 2005. The organization of the core proteins of the yeast spindle pole body. *Mol. Biol. Cell.* 16:3341–3352. http://dx.doi.org/10.1091/mbc.E05-03-0214

Paoletti, A., N. Bordes, R. Haddad, C.L. Schwartz, F. Chang, and M. Bornens. 2003. Fission yeast cdc31p is a component of the half-bridge and controls SPB duplication. *Mol. Biol. Cell.* 14:2793–2808. http://dx.doi.org/10.1091/mbc.E02-10-0661

Pereira, G., U. Grueneberg, M. Knop, and E. Schiebel. 1999. Interaction of the yeast gamma-tubulin complex-binding protein Spc72p with Kar1p is essential for microtubule function during karyogamy. *EMBO J.* 18:4180–4195. http://dx.doi.org/10.1093/emboj/18.15.4180

Robbins, E., and N.K. Gonatas. 1964. The ultrastructure of a mammalian cell during the mitotic cycle. *J. Cell Biol.* 21:429–463. http://dx.doi.org/10.1083/jcb.21.3.429

Rosenberg, J.A., G.C. Tomlin, W.H. McDonald, B.E. Snydsman, E.G. Muller, J.R. Yates III, and K.L. Gould. 2006. Ppc89 links multiple proteins, including the septation initiation network, to the core of the fission yeast spindle-pole body. *Mol. Biol. Cell.* 17:3793–3805. http://dx.doi.org/10.1091/mbc.E06-01-0039

Rüthnick, D., and E. Schiebel. 2016. Duplication of the yeast spindle pole body once per cell cycle. *Mol. Cell. Biol.* 36:1324–1331. http://dx.doi.org/10.1128/MCB.00048-16

Samejima, I., P.C. Lourenço, H.A. Snaith, and K.E. Sawin. 2005. Fission yeast mto2p regulates microtubule nucleation by the centrosomin-related protein mto1p. *Mol. Biol. Cell.* 16:3040–3051. http://dx.doi.org/10.1091/mbc.E04-11-1003

Samejima, I., V.J. Miller, L.M. Groocock, and K.E. Sawin. 2008. Two distinct regions of Mto1 are required for normal microtubule nucleation and efficient association with the gamma-tubulin complex in vivo. *J. Cell Sci.* 121:3971–3980. http://dx.doi.org/10.1242/jcs.038414

Samejima, I., V.J. Miller, S.A. Rincon, and K.E. Sawin. 2010. Fission yeast Mto1 regulates diversity of cytoplasmic microtubule organizing centers. *Curr. Biol.* 20:1959–1965. http://dx.doi.org/10.1016/j.cub.2010.10.006

Schaerer, F., G. Morgan, M. Winey, and P. Philippsen. 2001. Cnm67p is a spacer protein of the *Saccharomyces cerevisiae* spindle pole body outer plaque. *Mol. Biol. Cell.* 12:2519–2533. http://dx.doi.org/10.1091/mbc.12.8.2519

Seybold, C., M. Elserafy, D. Rüthnick, M. Ozboyaci, A. Neuner, B. Flottmann, M. Heilemann, R.C. Wade, and E. Schiebel. 2015. Kar1 binding to Sfi1 C-terminal regions anchors the SPB bridge to the nuclear envelope. *J. Cell Biol.* 209:843–861. http://dx.doi.org/10.1083/jcb.201412050

Stafstrom, J.P., and L.A. Staehelin. 1984. Dynamics of the nuclear envelope and of nuclear pore complexes during mitosis in the *Drosophila* embryo. *Eur. J. Cell Biol.* 34:179–189.

Su, S.S., Y. Tanaka, I. Samejima, K. Tanaka, and M. Yanagida. 1996. A nitrogen starvation-induced dormant G0 state in fission yeast: The establishment from uncommitted G1 state and its delay for return to proliferation. *J. Cell Sci.* 109:1347–1357.

Tallada, V.A., K. Tanaka, M. Yanagida, and I.M. Hagan. 2009. The *S. pombe* mitotic regulator Cut12 promotes spindle pole body activation and integration into the nuclear envelope. *J. Cell Biol.* 185:875–888. http://dx.doi.org/10.1083/jcb.200812108

Tanaka, K., and T. Kanbe. 1986. Mitosis in the fission yeast *Schizosaccharomyces pombe* as revealed by freeze-substitution electron microscopy. *J. Cell Sci.* 80:253–268.

Tang, N., and W.F. Marshall. 2012. Centrosome positioning in vertebrate development. *J. Cell Sci.* 125:4951–4961. http://dx.doi.org/10.1242/jcs.038083

Tomlin, G.C., J.L. Morrell, and K.L. Gould. 2002. The spindle pole body protein Cdc11p links Sid4p to the fission yeast septation initiation network. *Mol. Biol. Cell.* 13:1203–1214. http://dx.doi.org/10.1091/mbc.01-09-0455

Uzawa, S., F. Li, Y. Jin, K.L. McDonald, M.B. Braunfeld, D.A. Agard, and W.Z. Cande. 2004. Spindle pole body duplication in fission yeast occurs at the G1/S boundary but maturation is blocked until exit from S by an event downstream of cdc10+. *Mol. Biol. Cell.* 15:5219–5230. http://dx.doi.org/10.1091/mbc.E04-03-0255

Vallen, E.A., M.A. Hiller, T.Y. Scherson, and M.D. Rose. 1992. Separate domains of KAR1 mediate distinct functions in mitosis and nuclear fusion. *J. Cell Biol.* 117:1277–1287. http://dx.doi.org/10.1083/jcb.117.6.1277

Vallen, E.A., W. Ho, M. Winey, and M.D. Rose. 1994. Genetic interactions between CDC31 and KAR1, two genes required for duplication of the microtubule organizing center in *Saccharomyces cerevisiae*. *Genetics.* 137:407–422.

Vardy, L., and T. Toda. 2000. The fission yeast gamma-tubulin complex is required in G(1) phase and is a component of the spindle assembly checkpoint. *EMBO J.* 19:6098–6111. http://dx.doi.org/10.1093/emboj/19.22.6098

Venkatram, S., J.J. Tasto, A. Feoktistova, J.L. Jennings, A.J. Link, and K.L. Gould. 2004. Identification and characterization of two novel proteins affecting fission yeast γ-tubulin complex function. *Mol. Biol. Cell.* 15:2287–2301. http://dx.doi.org/10.1091/mbc.E03-10-0728

Venkatram, S., J.L. Jennings, A. Link, and K.L. Gould. 2005. Mto2p, a novel fission yeast protein required for cytoplasmic microtubule organization and anchoring of the cytokinetic actin ring. *Mol. Biol. Cell.* 16:3052–3063. http://dx.doi.org/10.1091/mbc.E04-12-1043

Wälde, S., and M.C. King. 2014. The KASH protein Kms2 coordinates mitotic remodeling of the spindle pole body. *J. Cell Sci.* 127:3625–3640. http://dx.doi.org/10.1242/jcs.154997

Winey, M., and K. Bloom. 2012. Mitotic spindle form and function. *Genetics.* 190:1197–1224. http://dx.doi.org/10.1534/genetics.111.128710

Wu, J.Q., J.R. Kuhn, D.R. Kovar, and T.D. Pollard. 2003. Spatial and temporal pathway for assembly and constriction of the contractile ring in fission yeast cytokinesis. *Dev. Cell.* 5:723–734. http://dx.doi.org/10.1016/S1534-5807(03)00324-1

Wu, Q., R. He, H. Zhou, A.C. Yu, B. Zhang, J. Teng, and J. Chen. 2012. Cep57, a NEDD1-binding pericentriolar material component, is essential for spindle pole integrity. *Cell Res.* 22:1390–1401. http://dx.doi.org/10.1038/cr.2012.61